



1 **Chronostratigraphic framework and provenance of the**
2 **Ossa-Morena Zone Carboniferous basins (SW Iberia)**

3

4 M. Francisco Pereira^{1*}, Cristina Gama¹, Ícaro Dias da Silva I.², José B. Silva³, Mandy
5 Hofmann⁴, Ulf Linnemann⁴, Andreas Gärtner⁴

6 1- Instituto de Ciências da Terra, Departamento de Geociências, ECT, Universidade de Évora, Apt.94,
7 7002-554 Évora, Portugal

8 2- Instituto Dom Luiz, Faculdade de Ciências da Universidade de Lisboa, Campo Grande, 1749-016
9 Lisboa, Portugal

10 3- Instituto Dom Luiz, Departamento de Geologia, Faculdade de Ciências da Universidade de Lisboa,
11 Campo Grande, 1749-016 Lisboa, Portugal

12 4- Senckenberg Naturhistorische Sammlungen Dresden, Museum für Mineralogie und Geologie,
13 Germany

14

15 Correspondence to: M. Francisco Pereira (mpereira@uevora.pt)

16

17 **Abstract.** Carboniferous siliciclastic and silicic magmatic rocks from the Santa Susana-São
18 Cristovão region contain valuable information regarding the timing of synorogenic processes in
19 SW Iberia. In this region of the Ossa-Morena Zone (OMZ), Late Carboniferous terrigenous
20 strata (i.e. the Santa Susana Formation) unconformably overlie Early Carboniferous marine
21 siliciclastic deposits alternating with volcanic rocks (i.e. the Toca da Moura volcano-
22 sedimentary complex). Lying below this intra-Carboniferous unconformity, the Toca da Moura
23 volcano-sedimentary complex is intruded and overlain by the Baleizão porphyry. Original
24 SHRIMP and LA-ICP-MS U-Pb zircon are presented in this paper, providing
25 chronostratigraphic and provenance constraints, since available geochronological information is
26 scarce and only biostratigraphic ages are currently available for the Santa Susana-São Cristovão
27 region. Our findings and the currently-available detrital zircon ages from Paleozoic terranes of
28 SW Iberia (Pulo do Lobo Zone- PLZ, South-Portuguese Zone- SPZ, and OMZ), were jointly
29 analyzed using the K-S test and MDS diagrams to investigate provenance. The marine
30 deposition is constrained to the age interval of c. 335-331 Ma (Viséan) by new U-Pb data for
31 silicic tuffs from the Toca da Moura volcano-sedimentary complex. The Baleizão porphyry,
32 intrusive in the Toca da Moura volcano-sedimentary complex, yielded a crystallization age of c.
33 317 Ma (Bashkirian), providing the minimum age for the overlying intra-Carboniferous
34 unconformity. A comparison of detrital zircon populations from siliciclastic rocks of the
35 Cabrela and Toca de Moura volcano-sedimentary complexes of the OMZ suggests that they



36 derived from distinct sources more closely associated with the SPZ and PLZ than the OMZ.
37 Above the intra-Carboniferous unconformity, the Santa Susana Formation is either the result of
38 the recycling of distinct sources located in the Laurussian-side (SPZ and PLZ) and Gondwanan-
39 side (OMZ) of the Rheic suture zone. The best estimate of the crystallization age of a granite
40 cobble found in a conglomerate from the Santa Susana Formation yielded c. 303 Ma
41 (Kasimovian-Gzhelian), representing the maximum depositional age for the terrestrial strata.
42 The intra-Carboniferous unconformity seems to represent a stratigraphic gap of approximately
43 12-14 Ma, providing evidence of the rapid post-accretion/collision uplift of the Variscan
44 orogenic belt in SW Iberia (i.e. the OMZ, PLZ and SPZ).

45

46 **1. Introduction**

47 U-Pb geochronology of detrital zircon from siliciclastic rocks has been extensively used in
48 stratigraphic correlation studies for estimating the maximum depositional age and investigating
49 the provenance of sedimentary sequences (Fedó et al., 2001; Dickinson and Gehrels, 2009). The
50 youngest detrital zircon grains found in siliciclastic rock commonly provide useful information
51 about depositional age, especially in areas that experienced active volcanism during sediment
52 accumulation (Gehrels, 2014). The maximum depositional age obtained for siliciclastic rock is
53 often not necessarily coincident with the biostratigraphic age as defined by key fossil
54 assemblages (Pereira et al., 2019). Therefore, in order to overcome any doubt about the true age
55 of deposition, it is desirable that volcanic rocks interstratified with fossiliferous siliciclastic
56 rocks should be dated (Fedó et al., 2001; Bowring et al., 2006). Furthermore, the application of
57 zircon U-Pb geochronology to volcano-sedimentary and sedimentary sequences that are
58 separated by unconformities, by means of the comparative analysis of their age populations,
59 may be useful for estimating time intervals and revealing changes in provenance. Volcanic
60 rocks that lie beneath or overlie sedimentary sequences and unconformities can provide
61 maximum and minimum ages, respectively. When detrital zircon geochronology is linked to the
62 geochronology of crosscutting younger igneous rocks, then both a maximum and minimum age
63 bracket for deposition can be determined (Fedó et al., 2001).

64 The Variscan orogen that extends from central Europe to Iberia was reworked through discrete
65 Carboniferous sedimentary cycles during the Laurussia-Gondwana convergence, giving rise to
66 the formation of marine and terrestrial basins. In SW Iberia, stratigraphic correlation has been
67 proposed for the Carboniferous synorogenic strata found in the three main tectonostratigraphic
68 divisions of the Variscan Orogen: the Ossa-Morena (OMZ), Pulo do Lobo (PLZ) and South
69 Portuguese (SPZ) zones (Quesada and Oliveira, 2019, and references therein).

70 The Carboniferous siliciclastic strata in the Santa Susana-São Cristovão region (OMZ) includes
71 fossils indicating Carboniferous to Kasimovian biostratigraphic ages (Teixeira, 1938-1940, 1941;
72 Lemos de Sousa and Wagner, 1983; Wagner and Lemos de Sousa, 1983; Pereira et al., 2006;



73 Machado et al., 2012; Lopes et al., 2014). In the Santa Susana-São Cristovão region, Late
74 Carboniferous siliciclastic strata of the Santa Susana Formation unconformably overlies: i) the
75 poorly-dated Baleizão volcanic-subvolcanic suite, and ii) the Early Carboniferous Toca da
76 Moura volcano-sedimentary complex, which includes volcanic rocks that have never been
77 dated. This intra-Carboniferous unconformity was generated as consequence of regional uplift
78 and falling sea level, leading to a change in depositional environment from Early Carboniferous
79 marine to Late Carboniferous terrestrial (Gonçalves and Carvalhosa, 1984; Oliveira et al., 1991;
80 Machado et al., 2012). The provenance of the above-mentioned Carboniferous strata has been
81 discussed based on petrographic, paleontological and detrital zircon geochronology evidence
82 (Pereira et al., 2006; Machado et al., 2012; Lopes et al., 2014; Dinis et al., 2018).
83 In this paper, SHRIMP and LA-ICP-MS U-Pb analyses were performed on zircon grains from
84 silicic volcanic, subvolcanic, and siliciclastic rocks sampled in the Santa Susana-São Cristovão
85 region (OMZ, SW Iberia). The aim of this geochronology study is to establish the
86 chronostratigraphic framework of the Carboniferous strata in the Santa Susana-São Cristovão
87 region and to discuss their provenance using a statistical approach (Kolmogorov-Smirnov test
88 and Mutiscaling diagrams). Thus we pay tribute to J.R. Martínez-Catalán, who devoted part of
89 his career to investigating the Carboniferous synorogenic basins of NW Iberia.

90

91 **2. Geological setting**

92 In SW Iberia, the tectonic limit between the OMZ (Gondwanan-side) and the PLZ and SPZ
93 (Laurussian-side) has been regarded as constituting the tectonically reworked suture zone of the
94 Rheic Ocean (Andrade, 1983; Quesada et al., 1994; Simancas et al., 2005; Díaz-Apiroz et al.,
95 2006; Ribeiro et al., 2007; Pereira et al., 2017a) (Fig. 1). This Paleozoic suture zone has been
96 defined along the Beja-Acebuches ophiolitic complex (Fonseca et al., 1999, and references
97 therein). The Beja-Acebuches ophiolitic complex is separated from the Beja Igneous Complex
98 (Jesus et al., 2007, 2016) by a strike-slip fault. Metabasalts and metagabbros (i.e. the Mombeja
99 unit of Andrade, 1983) from the Beja-Acebuches ophiolitic complex have been dated at c. 340-
100 332 Ma (U-Pb zircon; Azor et al., 2008), while in the Beja Igneous Complex gabbro and
101 granitic rocks are relatively older, yielding crystallization ages of c. 353-342 Ma (U-Pb zircon;
102 Jesus et al., 2007; Pin et al., 2008). Trace element and isotopic signatures of Beja Igneous
103 Complex plutonic rocks indicate crustal contamination of parental magmas deriving from a
104 depleted asthenospheric mantle reservoir (Santos et al., 1990; Pin et al., 2008; Jesus et al.,
105 2016). The plutonic rocks of the Beja Igneous Complex show well-defined intrusive contacts
106 with previously deformed and metamorphosed sedimentary and igneous rocks of the OMZ
107 basement (Rosas et al., 2008; Pin et al., 2008). The Beja Igneous Complex also includes the São
108 Cristovão-Alcáçovas subvolcanic complex (Gonçalves and Carvalhosa, 1984), composed of
109 silicic sub-volcanic and volcanic rocks (i.e. the Baleizão unit of Andrade, 1983), granophyres



110 and porphyries dated at c. 324 Ma (K-Ar on biotite; Priem et al., 1986), associated with
111 diabases. The major and trace element geochemistry of the Baleizão porphyries indicates a calc-
112 alkaline rhyolitic, rhyodacitic and andesitic composition typical of magmas produced at
113 convergent plate boundaries (Santos et al., 1987; Caldeira et al., 2007; Ferreira et al., 2014). The
114 Baleizão porphyries occur as dykes and sills (Andrade, 1927) (Figs. 3a, b), overlying
115 (Gonçalves and Carvalhosa, 1984) the Early Carboniferous siliciclastic and volcanic rocks of
116 the Toca da Moura volcano-sedimentary complex (Santos et al., 1987, and references therein)
117 (Fig. 2).

118 The Toca da Moura volcano-sedimentary complex is mainly composed of pelites (i.e.
119 “Xistinhos”; Teixeira, 1944; Fig. 3a) and greywackes, associated with andesite-to-rhyolite
120 volcanic rocks (lava flow and tuffs; Figs. 3c, d, e), andesitic basalt (Fig. 3f), chert layers
121 (Gonçalves and Carvalhosa, 1984), and a few olistoliths of basalt and limestone. Siliciclastic
122 rocks contain well-preserved in-situ palynomorph assemblages of Tournaisian to Visean age
123 and reworked palynomorphs ranging in age from the Middle Cambrian to the Early Tournaisian
124 (Pereira et al., 2006; Lopes et al., 2014). Based on geochemical information, this volcanism was
125 interpreted by Santos et al. (1987) as deriving from calc-alkaline magma produced in a
126 continental magmatic arc. A stratigraphic correlation was established between the Toca da
127 Moura volcano-sedimentary complex and the Cabrela volcano-sedimentary complex (Pereira et
128 al., 2006) which is located 15 km to the NW, in the Évora Massif (Pereira et al., 2007; 2012a)
129 (Fig. 1b). The presence of variable-scale soft-sediment structures (i.e. slumps, intraclast
130 conglomerates and olistoliths) in both complexes indicates gravity-induced instability during
131 marine sedimentation. Detrital zircon ages of a siliciclastic rock from the Cabrela volcano-
132 sedimentary complex are mainly Middle-Late Devonian (82%) and Early Carboniferous (14%),
133 also including a few older grains (sample OM-200 from Pereira et al., 2012a).

134 The Santa Susana Formation (i.e. Santa Susana basin, Domingos et al., 1983; Quesada et al.,
135 1990, Oliveira et al. 1991) siliciclastic rocks that outcrop along a NNW-SSE-trending narrow
136 discontinuous band which is 0.1-5 km wide and 12 km long unconformably overlie the Baleizão
137 Porphyry and the Toca da Moura volcano-sedimentary complex (Fig. 2), forming the geological
138 contact between these stratigraphic units often defined by faults (Gonçalves and Carvalhosa,
139 1984). The Santa Susana Formation is divided into two members (Machado et al., 2012, and
140 references therein): i) the lower member is mainly composed of coarse-grained sandstone and
141 conglomerate beds (Figs. 4a, b, c, d); these conglomerates include pebbles and cobbles of silicic
142 porphyry, rhyolite, andesite, basalt, granite, felsic tuff, pelite, sandstone, greywacke, quartzite,
143 phyllite, chert, and quartz (Figs. 4e, f); ii) the upper member represents a repetitive sequence of
144 alternating beds of pelite and sandstone interbedded with coal seams, and few beds of
145 conglomerate (Fig. 2). These terrestrial deposits were most probably deposited in an
146 alluvial/fluviol-to-fluvial/lacustrine (floodplain lakes and/or abandoned channels with abundant



147 vegetation) system. The plant fossils identified in the siliciclastic rocks of the Santa Susana
148 Formation indicate a Moscovian-Kasimovian biostratigraphic age (Wagner and Lemos de
149 Sousa, 1983). Pelitic beds from the Upper member include palynomorph assemblages assigned
150 with Kasimovian age (Machado et al., 2012). Palynomorphs ranging in age from the middle
151 Cambrian to the early Moscovian were also found in siliciclastic rocks of the Santa Susana
152 Formation sampled from a borehole at a depth of around 400 m (Lopes et al., 2014). Detrital
153 zircon ages from upper member sandstones (Dinis et al., 2018) are mainly distributed over
154 Devonian–Carboniferous (41–51%), Paleoproterozoic (23–30%) and Ediacaran–Cryogenian (16–
155 23%) groups, and also a few Stenian–Tonian and Archean grains.

156

157 **3. Rational and analytical methods**

158 In this study, SHRIMP U-Pb analyses were performed for the first time on magmatic zircon
159 from two samples of tuff from the Toca da Moura volcano-sedimentary complex (TM-1 and
160 SCV-2; Figs. 3c, d), one from the Baleizão silicic porphyry (SCV-30; Fig. 3b), and a cobble of
161 granite (SCV-7; Fig. 4e) found in a conglomerate from the lower member of the Santa Susana
162 Formation. Estimations of the crystallization age of samples SCV-2 and TM-1 (syndepositional
163 volcanism), and sample SCV-30 (post-depositional) were used to validate the Tournaisian-
164 Viséan biostratigraphic age previously attributed to the Toca da Moura volcano-sedimentary
165 complex based on palynological assemblages (Pereira et al., 2006; Lopes et al., 2014). The
166 presence of granite cobbles and pebbles in conglomerate layers from the lower Santa Susana
167 Formation indicates denudation and recycling of a crystalline basement involving granite whose
168 age is unknown. The dating of the granite cobble (sample SCV-7) is useful for discussing
169 provenance and estimating the maximum depositional age of the Santa Susana conglomerate. In
170 addition, LA-ICP-MS U-Pb analyses were performed on detrital zircon grains from two samples
171 of sandstone from the upper and lower members of the Santa Susana Formation (samples SS-1
172 and SS-2, respectively; Fig. 5g, h), and a sample of pelite from the Toca da Moura volcano-
173 sedimentary complex (sample TM-3; Fig. 5e). This new U-Pb data is useful for discussing
174 provenance and determining the maximum depositional ages of the two sedimentary sequences
175 separated by an intra-Carboniferous unconformity. Sample locations in the Santa Susana-São
176 Cristovão region are indicated in Figure 2. Finally, detrital zircon grains of siliciclastic rock
177 from the Cabrela volcanic-sedimentary complex (sample CBR-11; Fig. 5f; equivalent to sample
178 OM-200 of Pereira et al. 2012a) were analyzed to test for the existence of pre-Devonian ages.
179 The new U-Pb results obtained in the present study are compared with previously-reported age
180 spectra for pre-Kasimovian siliciclastic rocks from the OMZ, PLZ and SPZ siliciclastic
181 sequences of SW Iberia, using statistical tools.

182 Zircon grains for U-Pb geochronology were selected using traditional techniques: density
183 separation using a wilfley table (Universidad Complutense de Madrid, Spain) and also using



184 granulometric separation using sieves with a mesh size of less than 500 microns, density
185 (panning) separation procedures, and mineral identification using a binocular lens and
186 preparation of epoxy resin mounts with zircon grains (Universidade de Évora, Portugal). U-Pb
187 measurements were obtained at IBERSIMS (Universidad de Granada, Spain) using SHRIMP,
188 and also at the Senckenberg Naturhistorische Sammlungen Dresden (Museum für Mineralogie
189 und Geologie, Germany) using a LA-ICP-MS. U-Pb measurements using SHRIMP and LA-
190 ICP-MS followed the procedures previously described by Dias da Silva et al. (2018) and Pereira
191 et al. (2012a), respectively. U-Pb results are listed in Tables S1 and S2 (Supplementary
192 Material). Concordia curves and weighted-average means were obtained using Isoplot 4
193 (Ludwig, 2003) (Figs. 6 and 7). Kernel density estimation (KDE) diagrams were produced with
194 90-110 % concordant $^{206}\text{Pb}/^{238}\text{U}$ ages for grains younger than 1.0 Ga, and $^{207}\text{Pb}/^{206}\text{Pb}$ ages for
195 older grains (for further details, see Frei and Gerdes, 2009) using IsoplotR (Vermeesch, 2018)
196 (Figs. 8a, b). Cathodoluminescence-imaging was performed at TU Bergakademie Freiberg
197 (Germany) and at IBERSIMS.

198 The K-S test and the MDS technique were used in conjunction to compare populations of
199 detrital zircon U-Pb ages obtained from the Carboniferous siliciclastic rocks of the Santa
200 Susana-São Cristovão region using a method designed for a recent study of the provenance of
201 Triassic sandstones (Gama et al., in press, and references therein). The K-S test is a non-
202 parametric statistical tool that has been successfully used for the comparison of two populations
203 of detrital zircon U-Pb ages by evaluating whether they are significantly different, i.e. indicating
204 whether zircon age populations correlate with a similar source or not, regardless of whether they
205 are of different sizes, while including at least 20 measurements (DeGraaff-Surpless et al., 2003).
206 The probability of the observed maximum vertical difference between the cumulative
207 probability curves (D-value; Fig. 7c) being unrelated to age differences between the two detrital
208 zircon populations is given by a P-value corresponding to a confidence interval of 95%
209 (Barbeau Jr. et al.; 2009; Guynn and Gehrels, 2010) (Fig. 9a). High P-values and low D-values
210 indicate that the observed difference between the two detrital zircon populations may be
211 explained by the existence of common sources (Gama et al., in press, and references therein). K-
212 S analyses were carried out using an Excel spreadsheet published on the University of Arizona
213 Geochronological Center website at <https://sites.google.com/a/laserchron.org/laserchron/>. The
214 MDS technique provides a means for the comparison of samples based on quantified pairwise
215 comparisons of their detrital zircon ages, and is extremely useful for visualising the degree of
216 similarity between samples in two dimensions, i.e. greater distances between samples represent
217 a greater degree of dissimilarity between points on MDS diagrams (Vermeesch, 2013; Spencer
218 and Kirkland, 2015; Wissink et al., 2018) (Fig. 9b). MDS diagrams were produced using
219 IsoplotR (Vermeesch, 2018).

220



221 **4. U-Pb geochronology: Results**

222 **4.1. Volcanic silicic rocks of the Toca da Moura volcano-sedimentary complex**

223 Sample SCV-2 is a fine-grained banded rhyolitic tuff consisting of variable size and shape
224 quartz and K-feldspar phenocryst and lithoclasts (less than 1mm in diameter) dispersed in ash
225 matrix (Fig. 5a). Zircon grains appear as stubby-to-elongated euhedral prisms (50-150 μm in
226 diameter), mostly showing oscillatory concentric zoning growing on distinct cores or as simple
227 crystals. There are some dark inclusions, unzoned patches and transgressive variably
228 luminescence embayments. A total of 44 U-Th-Pb SHRIMP analyses of 44 grains yielded U
229 content ranging from 262 to 628 ppm, and Th/U ratios ranging from 0.17 to 0.95 (mean = 0.42).
230 A group of 23 grains with $^{206}\text{Pb}/^{238}\text{U}$ ages (discordance $\leq 5\%$) yielded a weighted mean
231 $^{208}\text{Pb}/^{238}\text{U}$ age of 331 ± 4 Ma (MSWD = 1.2; Fig. 6a), which probably represents the
232 crystallization age of tuff.

233 Sample TM-1 is a fine-grained banded rhyolitic tuff consisting quartz, K-feldspar and biotite
234 phenocrysts, flattened dark-brown pumice (i.e. fiamme) and lithoclasts (less than 1mm in
235 diameter) enclosed in ash matrix (Fig. 5b). The zircon population is characterized by stubby
236 euhedral-to-sub-euhedral small (30-100 μm in diameter) grains. Magmatic grains are either
237 simple with concentric zoning or composite showing variably luminescence cores with
238 concentric zoning, unzoned, or banded zoned. These cores are surrounded by overgrowths with
239 concentric zoning and are occasionally diffuse or unzoned. A total of 120 U-Th-Pb LA-ICP-MS
240 analyses yielded U content ranging from 87 to 4136 ppm, and Th/U ratios ranging from 0.04 to
241 2.29 (mean = 0.53). 28 $^{206}\text{Pb}/^{238}\text{U}$ ages (90-110% of concordance) yield a weighted mean
242 $^{208}\text{Pb}/^{238}\text{U}$ age of 341 ± 10 Ma with a very poor fit (MSWD = 6.9; Fig. 6b), as indicated by the
243 scattering of ages along the Concordia curve. A coherent group of 21 grains with $^{206}\text{Pb}/^{238}\text{U}$ ages
244 yielded a weighted mean $^{208}\text{Pb}/^{238}\text{U}$ age of 335 ± 6 Ma (MSWD = 1.5; Fig. 6b), providing the
245 best age estimate for the volcanic rock (Fig. 6b). The youngest zircon grain (c. 302 Ma)
246 probably experienced Pb loss. The six oldest zircon grains present Paleoproterozoic (c. 2 Ga),
247 Neoproterozoic (c. 715 Ma) and Devonian (c. 395-378 Ma) ages, suggesting inheritance.

248

249 **4.2. Baleizão porphyry**

250 Sample SCV-30 is a porphyritic rhyodacite-rhyolite consisting of quartz, plagioclase, K-
251 feldspar, biotite and amphibole phenocryst (less than 3mm in diameter) embedded in a fine-
252 grained silicic matrix (Fig. 5c). The zircon population contains grains (30-120 μm in diameter)
253 from subrounded subhedral to prismatic euhedral. Prisms are equant to moderately elongate
254 showing simple internal structure characterized by concentric and sector zoning to unzoned. A
255 concentric zoned or unzoned rim surrounds unzoned cores of few composite grains. A total of
256 20 U-Th-Pb SHRIMP analyses for sample SCV-30 yielded U content ranging from 267 to 581
257 ppm, and Th/U ratios ranging from 0.34 to 0.52 (mean = 0.41). 15 analyses were obtained for



258 zircon with discordance $\leq 5\%$, distributed along the concordia curve from ca. 355 to 312 Ma,
259 and yielded a weighted mean $^{208}\text{Pb}/^{238}\text{Th}$ age of 332 ± 9 Ma (mean square of weighted deviates,
260 MSWD = 4.3; Fig. 7b). Some of the spread observed could be due to the presence of
261 inheritance. Five grains in the age range ca. 334-312 Ma yielded a weighted mean $^{208}\text{Pb}/^{238}\text{U}$ age
262 of 317 ± 12 Ma (MSWD = 2.1; Fig. 7a), which is regarded as the best estimate for the
263 crystallization age of subvolcanic silicic rock. The remaining oldest 10 grains yielded $^{206}\text{Pb}/^{238}\text{U}$
264 ages of c. 355-337 Ma which probably indicates inheritance.

265

266 **4.3. Cobble of granite found in a conglomerate from the Santa Susana Formation**

267 Sample SCV-7 is a cobble (20 cm in diameter) of pinkish medium-grained granite consisting of
268 quartz, alkali feldspar and biotite (Fig. 5d). Most zircons are stubby and elongated subeuhedral
269 to euhedral prisms (80 to 150 μm in diameter). Morphologically zircon grains are mostly simple
270 showing concentric zoning, sector zoning to unzoned, and few are composite with irregular and
271 unzoned small cores surrounded by a rim with concentric zoning. 40 U-Th-Pb SHRIMP
272 analyses were performed on sample SCV-7 with U content ranging from 348 to 3177 ppm, and
273 Th/U ratios ranging from 0.3 to 1.25 (mean = 0.5). Of this total of analyses 24 U-Pb ages with
274 discordance $\leq 5\%$, scattered along the concordia curve from ca. 349 to 294 Ma, yielded a
275 weighted mean $^{206}\text{Pb}/^{238}\text{U}$ age of 327 ± 7 Ma (MSWD = 4; Fig. 7b). A group of six zircon grains
276 in the age range of c. 309-294 Ma yielded a weighted mean $^{206}\text{Pb}/^{238}\text{U}$ age of 303 ± 6 Ma
277 (MSWD = 0.98; Fig. 7b), which is taken as the probable crystallization age of the granite. The
278 remaining 19 zircon grains yielded $^{206}\text{Pb}/^{238}\text{U}$ ages of c. 349-326 Ma, suggesting inheritance.

279

280 **4.4. Siliciclastic rocks from the Toca da Moura and Cabrela volcano-sedimentary** 281 **complexes**

282 Sample TM-3 is a laminated poorly-sorted siltstone with quartz-rich silt layers, containing
283 feldspar and tourmaline grains, and lithoclasts (Fig. 5e), which are intercalated with darker
284 layers of clay. The zircon population is mostly characterized by stubby to elongated prismatic
285 small grains (less than 100 μm in diameter). It includes simple and composite zircons showing
286 concentric, sector and banded zoning. Of a total of 82 U-Th-Pb LA-ICP-MS analyses, with U
287 content ranging from 19 to 4630 ppm, and Th/U ratios ranging from 0.01 to 4.53 (mean = 0.75),
288 36 zircon grains yield 90-110% concordance. The Paleozoic population of detrital zircon (36%)
289 includes Early Carboniferous (9%, c. 353, 349 and 340 Ma), Ordovician (14%, c. 476-456 Ma),
290 Cambrian (7%, c. 531-500 Ma) and Late Devonian (6%, c. 369 and 362 Ma) grains (Fig. 8a).
291 The Precambrian population (64%) is predominantly Neoproterozoic (36%; c. 983-587 Ma), but
292 also includes Paleoproterozoic (14%; c. 2-1.8 Ga), Mesoproterozoic (8%; c. 1.3-1 Ga) and
293 Archean (6%; c. 2.7-2.5 Ga) grains. The three youngest zircon grains (c. 353-340 Ma) yielded a
294 maximum depositional age of c. 348 Ma (Tournaisian), which is in accordance with the



295 sedimentary age inferred from biostratigraphic constraints (Late Tournaisian to Middle-Late
296 Viséan; Pereira et al., 2006; Lopes et al., 2014).
297 Sample CBR-11 is a fine-grained poorly-to-moderate sorted siltstone consisting predominantly
298 of quartz and few feldspar grains and lithoclasts enclosed in silt-clay-sized particles (Fig. 5g).
299 Most of zircon grains are small (less than 100 μm in diameter), euhedral to subeuhedral. They
300 are simple grains (short, stubby to equant prisms) with oscillatory concentric and banded
301 zoning, and only few are composite grains with rounded cores. Of a total of 20 U-Th-Pb LA-
302 ICP-MS analyses, with U content ranging from 54 to 1379 ppm, and Th/U ratios ranging from
303 0.2 to 1.69 (mean = 0.81), 10 grains yielded 90-110% of concordance. Five grains are Paleozoic
304 (Carboniferous: c. 359, 351 and 346 Ma; Cambrian: c. 514 and 511 Ma) and five are
305 Precambrian (Paleoproterozoic: c. 2.4, 2.1 and 1.8 Ga; Mesoproterozoic: 1 Ga; Neoproterozoic:
306 c. 603 Ma). By combining our new data with those from sample OM-200 (Pereira et al., 2012a),
307 it was found that the detrital zircon population (CB; Fig. 8a) is largely dominated by Paleozoic
308 grains (90%): Late-Middle Devonian (68%), Early Carboniferous (15%), Cambrian (4%) and
309 Early Devonian (2%) grains, being distinct from sample TM-3 described above (Fig. 8a). The
310 youngest zircon population (N = 5; c. 353-346 Ma) yielded a weighted mean age of c. 351 Ma
311 (Tournaisian), suggesting a maximum depositional age which is slightly older than the
312 sedimentary age inferred from biostratigraphic constraints (Late Tournaisian to Middle-Late
313 Viséan; Pereira et al., 2006).

314

315 **4.5. Siliciclastic rocks from the Santa Susana Formation**

316 Sample SS-2 represents medium-to-coarse grained poorly-sorted sandstone. It is mainly
317 composed of lithoclasts (siltstone, mudstone, quartzite, phyllite, rhyolite, basalt) and quartz
318 grains, but also includes muscovite and feldspar grains (Fig. 5g). The zircon population is
319 mostly characterized by stubby to prismatic, subrounded to subangular, grains (120-300 μm in
320 diameter). Morphologically were found simple and composite grains. Cathodoluminescence
321 imaging shows that most zircon grains have concentric oscillatory zoning, irregular zoning and
322 are banded or unzoned. A total of 153 U-Th-Pb LA-ICP-MS analyses were performed on
323 detrital zircon grains. They show U content ranging from 15 to 6158 ppm, and Th/U ratios
324 ranging from 0.02 to 3.57 (mean = 0.66). A population with 51 grains yielding U-Pb ages with
325 90-110% concordance (Fig. 8b) is dominated by Precambrian ages (64%): Neoproterozoic
326 (37%; c. 801-551 Ma), Paleoproterozoic (25%; c. 2.4-1.6 Ga) and Neorchean (2%, c. 2.5 Ga).
327 The Paleozoic grains (36%) are Carboniferous (20%; c. 359-303 Ma), Late Devonian (14%; c.
328 378-362 Ma), and Early Ordovician (2%; c. 447 Ma). The youngest grain (c. 303 Ma;
329 Kasimovian-Gzhelian) is slightly younger than the sedimentary age inferred from
330 biostratigraphic constraints (Middle Moscovian to Kasimovian; Lemos de Sousa and Wagner,
331 1983; Machado et al., 2012; Lopes et al., 2014).



332 Sample SS-1 represents a very-coarse grained sandstone consisting of rounded-to-subangular
333 mono- and polycrystalline quartz, feldspar and muscovite grains, and a wide variety of
334 lithoclasts (chert, phyllite, rhyolite, siltstone and sandstone; Fig. 5h) . Zircon grains are rounded
335 to subangular, stubby and elongated prisms (less than 280 μm in diameter). The zircon
336 population includes simple grains with oscillatory concentric, banded and sector zoning, and
337 composite grains with cores with distinct internal morphologies surrounded by variable width
338 rims. A total of 150 U-Th-Pb LA-ICP-MS analyses performed on detrital zircon grains yielded
339 U content ranging from 24 to 9819 ppm, and Th/U ratios ranging from 0.05 to 2.89 (mean =
340 0.72). A group of 71 grains yielding U-Pb ages with 90-110% concordance are dominated by
341 Paleozoic ages (82%), predominantly made up of Carboniferous (49%; c. 358-315 Ma) and
342 Devonian (25%; c. 389-359 Ma), and a few Late Ordovician-Silurian (5%; c. 434, 429 and 425
343 Ma) and Cambrian (3%; c. 533 and 491 Ma) grains (Fig. 8b). The Precambrian grains (18%) are
344 Neoproterozoic (10%; c. 702-542 Ma), Paleoproterozoic (4%; c. 2.1-1.6 Ga), Mesoproterozoic
345 (3%, c. 1.4 and 1.6 Ga) and Neorchean (1%, c. 2.8 Ga). The youngest zircon population ($N = 3$;
346 c. 319-315 Ma) yielded a maximum depositional age of c. 316 Ma (Bashkirian-Moscovian),
347 which is slightly older than the sedimentary age inferred from biostratigraphic constraints
348 (Middle Moscovian to Kasimovian; Lemos de Sousa and Wagner, 1983; Machado et al., 2012;
349 Lopes et al., 2014).

350

351 **5. K-S test and MDS analysis: results**

352 The K-S test performed on the Santa Susana sandstones show that the detrital zircon
353 populations of sample SS-2 (lower member) and SS upper member (i.e. includes samples StS2
354 and StS4 from Dinis et al., 2018) are ‘not significantly different’ (all ages- P-value = 0.169;
355 pre-Carboniferous ages- P-value = 0.879) at the 5% confidence level (Fig. 9a). A comparison of
356 samples SS-1 and SS-2 reveals that they are “significantly different” (P-value ≤ 0.01). Unlike
357 sample SS-2, the sample SS-1 detrital zircon population is “significantly different” (P-value $<$
358 0.01) from the SS upper population (Fig. 9a), indicating distinct sources. Besides this, sample
359 SS-1 is much closer to that of the SS upper (D-value = 0.323), and more distant from sample
360 SS-2 (D-value = 0.465) as regards the distance between cumulative probability curves (Fig. 8c).
361 In Figure 9b, the MDS diagram produced with all ages shows sample SS-1 adjacent to Cabrelas
362 and Mértola siliciclastic rocks, while sample SS-2 is near the Mira, Santa Iria and Represa
363 detrital zircon populations. In the MDS diagram for pre-Carboniferous ages, sample SS-2 is
364 juxtaposed with sample TM-3, and closest to the Mira, Phyllite-Quartzite and Tercenas
365 formations (Fig. 9c) suggesting likely sources. Nevertheless, the probable contribution to SS-2
366 samples of sediment derived from the oldest siliciclastic rocks from the PLZ and SPZ (i.e. Pulo
367 do Lobo, Gafo, Ribeira de Limas, Atalaia and Ronquillo formations), and OMZ sources cannot
368 be excluded. Their detrital zircon populations are ‘not enough significantly different’ (all ages-



369 P-value = 0.003), and ‘not significantly different’ (pre-Carboniferous ages- P-value = 0.113-
370 0.165) at the 5% confidence level (Fig. 9a). This similarity is also illustrated in the
371 approximation between SS-2, P-G-R-A-R and OMZ populations in the MDS diagrams (Figs.
372 9b, c).
373 K-S test results for the comparison between samples SS-2 and TM-3 indicate that they present
374 ‘not significantly different’ detrital zircon populations (all ages- P-value = 0.399; pre-
375 Carboniferous ages- P-value = 0.0411) at the 5% confidence level (Fig. 9a). Furthermore, their
376 cumulative probability curves are much closer (Fig. 8d): D-values are 0.195 (all ages) and 0.203
377 (pre-carboniferous ages) (Fig. 9a). The close relationship of the two detrital zircon populations
378 suggests that the Toca da Moura volcano-sedimentary complex directly supplied sediment to the
379 Santa Susana basin. However, the relationship described above does not extend to the entire
380 Santa Susana basin since sample SS-1 presents a greater degree of similarity with the Cabrela
381 detrital zircon population as regards the proximity between cumulative probability curves (Fig.
382 8d) and MDS diagrams (Figs. 9b, c).
383 In addition, Cabrela siliciclastic rocks are ‘significantly different’ at the 5% confidence level
384 from sample TM-3 (P-values < 0.01) as regards the significant distance between them on the
385 MDS diagram (Figs. 9b, c), and the significant distance between cumulative curves (Fig. 8d),
386 with a D-value interval of 0.712-0.731 (Fig. 9a). The difference found in the detrital zircon
387 populations suggests that Cabrela and Toca da Moura siliciclastic rocks probably derived from
388 different sources.
389 As result of the K-S test and MDS analysis, the Horta da Torre Formation is ‘significantly
390 different’ (Fig. 9a), and is clearly separate (Figs. 9b, c) from all the other detrital zircon
391 populations, ruling out the possibility of it being a source for the Toca da Moura and Cabrela
392 volcano-sedimentary complexes or Santa Susana Formation siliciclastic rocks.

393

394 **6. Discussion**

395 **6.1. Chronostratigraphic framework**

396 The geochronological data presented in the present study provide the basis for the first
397 chronostratigraphic record for the Carboniferous basins of the Santa Susana-São Cristóvão
398 region (SW Iberia). Dating of silicic volcanic rocks interbedded in the Toca da Moura volcano-
399 sedimentary complex constrain an interval of felsic magmatism to occurring from c. 335 Ma to
400 331 Ma (Viséan; Fig. 6), complementing currently-available biostratigraphic information for
401 Toca da Moura siliciclastic rocks (Pereira et al., 2006; Lopes et al., 2014). U-Pb ages of the
402 youngest detrital zircon grains from the siliciclastic rocks of the Toca da Moura and Cabrela
403 volcano-sedimentary complexes (TM-3 and CB, respectively; Fig. 8a) provide maximum age
404 constraints for these marine deposits. Their maximum depositional ages (c. 351-348 Ma;
405 Tournaisian) are slightly older than currently-available biostratigraphic ages (Pereira et al.,



406 2006; Lopes et al., 2014), but provide confirmation that both marine deposits are broadly
407 contemporaneous.
408 Furthermore, the best estimate of the crystallization age of the Baleizão silicic intrusion
409 provides a minimum age of c. 317 Ma (Bashkirian; Fig. 7a) for the intra-Carboniferous
410 unconformity. Zircon extracted from a pebble of granite found in a Santa Susana conglomerate
411 yielded a crystallization age of c. 303 Ma for plutonic rock (Fig. 7b). This age estimate overlaps
412 the age interval of c. 305-303 Ma (i.e. the maximum depositional age range) obtained for the
413 youngest population of detrital zircon grains from sandstone of the upper member (Dinis et al.,
414 2018), complementing the currently-available biostratigraphic information for the Santa Susana
415 Formation (Machado et al., 2012; Lopes et al., 2014). Given the findings described above, a
416 stratigraphic interval of approximately 12-14 Ma can be established for the intra-Carboniferous
417 unconformity, marking a change in depositional environment from marine to terrestrial in the
418 OMZ. Basin-drainage and infill patterns most probably changed due to rapid uplift of the
419 Variscan-Appalachian orogenic belt, active during the waning stages of Laurussia-Gondwana
420 collision (i.e. Late Carboniferous).

421

422 **6.2. Provenance and evolutionary model**

423 An initial important finding based on the comparison of detrital zircon populations of Viséan
424 siliciclastic rocks from the Toca da Moura and Cabrela volcano-sedimentary complexes
425 provides evidence that they derived from different sources. The TM-3 population presents 64%
426 Precambrian detrital zircon grains, while the CB population contains only 10% (Fig. 8a). Toca
427 da Moura siliciclastic rocks have a greater affinity with the Phyllite-Quartzite, Tercenas, Santa
428 Iria and Represa formations (Fig. 9), indicating that detrital zircon populations were reproduced
429 faithfully in SPZ and PLZ (Laurussian-type) sources. A contribution from the oldest siliciclastic
430 sequences of PLZ (Pulo do Lobo, Atalaia, Gafo and Ribeira de Limas formations) and OMZ
431 (Gondwanan-type) sources cannot be ruled out for sample TM-3 (Fig. 9). The number of Late-
432 Middle Devonian zircon grains in sample TM-3 (6%) is smaller than that of the CB population
433 (68%) (Fig. 8a), suggesting that Cabrela siliciclastic rocks were most likely derived largely from
434 a Devonian source consistent with a limited contribution from recycled ancient rocks. This
435 indicates that the origin of the Viséan Toca da Moura and Cabrela basins is most likely more
436 closely linked to sources located in the SPZ and PLZ (Laurussian-type) than in the OMZ
437 (Gondwanan-type). The evidence in the Viséan Toca da Moura basin for dissection of the
438 inactive Devonian magmatic arc and the erosion of its plutonic roots, together with the recycling
439 of the PLZ and SPZ Frasnian-Tournaisian siliciclastic sequences and OMZ basement rocks,
440 differs from the evidence in the Cabrela basin. The significance of the involvement of distinct
441 sources is that part of the region located on the boundary between the OMZ- PLZ and the SPZ
442 (SW Iberia) was subjected to uplift while the remaining part underwent flexural subsidence. A



443 similar tectonic setting has been put forward as an explanation for differences in stratigraphy
444 found in the Pedroches syn-orogenic basin located along the OMZ-Central Iberian Zone
445 boundary (Armendáriz et al., 2008, and references therein) (Fig. 1). In the Visean, following the
446 closure of the Rheic Ocean (i.e. subduction beneath the Laurussian margin up to the end of
447 Devonian; Pérez-Cáceres et al., 2015; Pereira et al., 2017a, and references therein),
448 sedimentation occurred simultaneously with igneous activity on both the Laurussian-side and
449 the Gondwanan-side (Pereira et al., 2012b-Tecton). The upwelling of the asthenosphere and the
450 underplating of mantle-derived magmas could have triggered partial melting of crustal materials
451 and the intra-orogenic extension, creating the right conditions for the onset of gneiss domes
452 (Pereira et al., 2009; Dias da Silva et al., 2018). The emplacement of voluminous magmatism
453 with a composition typical of magmas produced, at convergent plate boundaries (Santos et al.,
454 1990; Jesus et al., 2007, 2016; Pin et al., 2008; Lima et al., 2012; Pereira et al., 2007, 2015a;
455 Moita et al., 2009, 2015), was simultaneously with flexural subsidence, marine sedimentation
456 and volcanism in the Visean (Pereira et al., 2012b) (Fig. 10a). A factor which may explain this
457 thermal anomaly is the subduction of an oceanic ridge beneath the OMZ (Gondwanan-side)
458 during the initial closure of the Paleotethys Ocean in the Carboniferous, whereas other regions
459 of the Appalachian-Variscan orogenic belt experienced oblique collision and rapid uplift
460 (Armendáriz et al., 2008; Pereira et al., in press), but as yet there is no consensus on this
461 (Simancas et al., 2009; Cambeses et al., 2015).

462 A second significant finding is that detrital zircon populations from the Santa Susana Formation
463 (samples SS-1 and SS-2) also show significant differences (Figs. 8 and 9). Basal conglomerate
464 (sample SS-2) presents a greater percentage of Precambrian grains (64%) than uppermost
465 sandstone (SS-1 sample; 28%), and presents a great degree of affinity with the detrital zircon
466 population of sample TM-3. Sample SS-2 presents a great degree of similarity with the detrital
467 zircon populations of overlying SS upper-member sandstones (samples StSz-2 and StSz-4;
468 Dinis et al., 2018) sampled as part of the same stratigraphic profile. SS-2 and SS upper-age
469 populations show a great degree of affinity (Fig. 9), suggesting that the two detrital zircon
470 grains were mainly derived from the erosion of the Toca da Moura volcano-sedimentary
471 complex, the Santa Iria and Represa formations (PLZ) and the Mira Formation (SPZ). However,
472 regarding the detrital zircon grains with pre-Carboniferous ages, additional contributions from
473 other PLZ (Pulo do Lobo, Atalaia, Gafo and Ribeira de Limas formations), SPZ (Brejeira,
474 Phyllite-Quartzite, Tercenas and Ronquillo formations) and OMZ sources cannot be ruled out
475 (Figs. 9a, c). The zircon age population of sample SS-1, which is distinct from the SS-2
476 population, presents a great degree of affinity with the CB population, suggesting lateral
477 changes in sources during deposition of Santa Susana uppermost sandstones. The great degree
478 of affinity of the SS-1, Cabrela volcano-sedimentary complex, with Mértola Formation detrital
479 zircon populations suggests a close association between the two and a common source. Cabrela



480 and Mértola siliciclastic rocks may be regarded as the main source for sample SS-1 and an
481 intermediate sediment repository as they are derived from the erosion of a Devonian source
482 partially represented by the Cercal porphyries from the SPZ. As result of rapid uplift, the
483 progressive erosion of the Devonian magmatic arc (including its plutonic roots), and that of
484 PLZ, SPZ and OMZ rocks, is evidenced in the Santa Susana Formation. The volumetrically
485 significant contribution of Carboniferous sources to the Santa Susana basin fill confirms
486 derivation from the erosion of: i) Pyrite Belt volcanic rocks, and Phyllite-Quartzite, Tercenas,
487 Mértola, Mira and Brejeira siliciclastic rocks (SPZ); ii) the Santa Iria and Represas formations
488 (PLZ); iii) Gil Marquez granitic rocks and other plutons of the Sierra del Norte Batholith (SPZ
489 and PLZ); iv) the Beja igneous complex, which includes the Baleizão porphyries (OMZ), and
490 Évora and Pavia plutonic and high-grade metamorphic rocks (OMZ); and v) the Cabrela and
491 Toca da Moura volcanic-sedimentary complexes (OMZ) and Mértola turbidites (SPZ). U-Pb
492 dating of magmatic zircon extracted from a pebble of granite (c. 303 Ma; Fig. 7b) found in a
493 conglomerate of the Santa Susana Formation lower member suggests provenance from the
494 direct erosion of Permo-Carboniferous plutons (i.e. original primary source), such as Santa
495 Eulália-Monforte granitic and gabbro-dioritic rocks (OMZ). This c. 303-297 Ma calc-alkaline
496 plutonic suite is coeval with the Nisa-Albuquerque and Los Pedroches batholiths, located on the
497 OMZ-Central Iberian Zone boundary (Fig. 1), probably representing a magmatic arc related to
498 the subduction of the Paleotethys Ocean (Pereira et al., 2015b, 2017b, in press). These Permo-
499 Carboniferous plutons were emplaced at shallow crustal levels consistent with the low
500 assimilation of country rocks and the sharp contacts, and therefore, they may have experienced
501 denudation shortly after its crystallization without being required unrealistic uplift rates.
502 In Kasimovian-Ghzelian, sedimentation probably occurred through the opening of the pull-apart
503 terrestrial basin related to the movement of major strike-slip faults (i.e. Porto-Tomar fault zone,
504 Machado et al., 2012, and references therein) during the waning stages of oblique continental
505 collision between Laurussia and Gondwana, simultaneously with the progressive uplift of the
506 Appalachian-Variscan orogenic belt (i.e. OMZ, PLZ and SPZ; Fig. 10b).

507

508 **7. Conclusions**

509 The main conclusions of this study are the following:

- 510 1. Viséan marine deposition in the Santa Susana-São Cristovão region is constrained to the age
511 interval of c. 335-331 Ma by the new U-Pb data for volcanic rocks intercalated within
512 siliciclastic rocks of the Toca da Moura volcano-sedimentary complex.
- 513 2. U-Pb dating of the Baleizão porphyry provides a minimum age of c. 317 Ma (Bashkirian) for
514 the overlying intra-Carboniferous unconformity.
- 515 3. Viséan siliciclastic rocks from the Cabrela and Toca de Moura volcano-sedimentary
516 complexes are derived from distinct sources, which probably include a Devonian continental



517 magmatic arc, and are likely to be more closely associated with the SPZ and PLZ (Laurussian-
518 type sources) than the OMZ (Gondwanan-type sources).
519 4. Terrestrial siliciclastic rocks from the Santa Susana Formation are probably the result of the
520 recycling of distinct sources associated with the SPZ, PLZ and OMZ.
521 5. The best estimate of crystallization of a granite pebble found in Santa Susana Formation
522 conglomerate yielded a maximum depositional age of ca. 303 Ma (Kasimovian-Gzhelian);
523 together with the youngest U-Pb ages (< c. 317 Ma) of detrital zircon grains, these findings
524 provide evidence of the denudation of primary crystalline sources during the rapid post-
525 accretion/collision uplift of the Variscan orogenic belt in SW Iberia (i.e. Gondwanan- and
526 Laurussian-type sources).
527 6. The intra-Carboniferous unconformity that separates the Toca da Moura volcano-complex
528 and the Baleizão porphyry from the Santa Susana Formation indicates a notable time interval of
529 approximately 12-14 Ma.

530

531 **Acknowledgements**

532 This work is a contribution to projects CGL2016-76438-P and PGC2018-096534-B-I00 (Spain),
533 the ICT's Research Group 6- Lithosphere Dynamics (ICT-UID/GEO/04683/2019) and, IDL's
534 Research Group 3- Solid Earth dynamics, hazards, and resources (Portuguese FCT). Í. Dias da
535 Silva acknowledges financial support by SYNTHESIS+ programme (2015-2016), FCT
536 postdoctoral grant SFRH/BPD/99550/2014 and FCT-project UID/GEO/50019/2019-IDL. This
537 is IBERSIMS publication number xx.

538

539 **References**

540 Andrade, A.S.: Contribution à l'Analyse de la Suture Hercynienne de Beja (Portugal), Perspectives
541 Métallogéniques. Unpublishe PhD thesis INPL, 137 p, 1983.
542
543 Andrade, C.F.: Alguns elementos para o estudo dos depósitos de carvão do Moinho da Ordem.
544 Comunicações dos Serviços Geológicos de Portugal, tomo XVI, 3-28, 1927.
545
546 Armendáriz, M., López-Guijarro, R., Quesada, C., Pin, C. and Bellido, F.: Genesis and evolution of a
547 syn-orogenic basin in transpression: Insights from petrography, geochemistry and Sm-Nd systematics in
548 the Variscan Pedroches basin (Mississippian, SW Iberia). *Tectonophysics* 461: 395-413, 2008.
549
550 Azor, A., Rubatto, D., Simancas, J.F., González Lodeiro, F., Martínez Poyatos, D., Martín Parra, L.M.
551 and Matas, J.: Rheic Ocean ophiolitic remnants in southern Iberia questioned by SHRIMP U-Pb zircon
552 ages on the Beja-Acebuches amphibolites. *Tectonics* 27, TC5006, doi:10.1029/2008TC002306, 2008.
553



- 554 Barbeau, D.L., Davis, J.T., Murray, K.E., Valencia, V., Gehrels, G.E., Zahid, K.M. and Gombosi, D.J.:
555 Detrital-zircon geochronology of the metasedimentary rocks of north-western Graham Land. *Antarctic*
556 *Science* 22, 65-78, 2009.
- 557
- 558 Bowring, S.A., Schoene, B., Crowley, J.L., Ramezani, J., Condon, D.J.: High-precision U-Pb zircon
559 geochronology and the stratigraphic record: Progress and promise. In: Olszewski, T. (Ed.),
560 *Geochronology: Emerging Opportunities*, Paleontological Society Short Course, October 21,
561 Philadelphia, PA., Paleontological Society Papers, Volume 11, 23-43, 2006.
- 562
- 563 Braid, J.A., Murphy, J.B., Quesada, C. and Mortensen, J.: Tectonic escape of a crustal fragment during
564 the closure of the Rheic Ocean: U-Pb detrital zircon data from the late Palaeozoic Pulo de Lobo and
565 South Portuguese Zones, Southern Iberia, *Journal of the Geological Society of London* 168, 383-392,
566 2011.
- 567
- 568 Caldeira, R., Ribeiro, M.L. and Moreira, M.E. Geoquímica das sequências máficas e félsicas entre Alvito,
569 Torrão e Alcáçovas (SW da ZOM). *Comunicações Geológicas*, 94, 5-28, 2007.
- 570
- 571 Cambeses, A., Scarrow, J.H., Montero, P., Molina, J.F. and Moreno, J.A. SHRIMP U-Pb zircon dating of
572 the Valencia del Ventoso plutonic complex, Ossa-Morena Zone, SW Iberia: Early Carboniferous intra-
573 orogenic extension-related 'calc-alkaline' magmatism. *Gondwana Research* 28, 735-756, 2015.
- 574
- 575 DeGraaff-Surplless, K., Mahoney, J.B., Wooden, J.L. and McWilliams, M.O.: Lithofacies control in
576 detrital zircon provenance studies: insights from the Cretaceous Methow Basin, Southern Canadian
577 Cordillera. *Geological Society of America Bulletin*, 115(8), 899-915, 2003.
- 578
- 579 Dias da Silva, Í., Pereira, M.F., Silva, J.B., and Gama, C.: Time-space distribution of silicic plutonism in
580 a gneiss dome of the Iberian Variscan Belt: The Évora Massif (Ossa-Morena Zone, Portugal).
581 *Tectonophysics* 747-748, 298-317, 2018.
- 582
- 583 Díaz Azpiroz, M., Fernandez, C., Castro, A. and El-Biad, M.: Tectonometamorphic evolution of the
584 Aracena metamorphic belt (SW Spain) resulting from ridge-trench interaction during Variscan plate
585 convergence. *Tectonics* 25, <http://dx.doi.org/10.1029/2004TC001742>, 2006.
- 586
- 587 Dickinson, W.R. and Gehrels, G.E.: Use of U-Pb ages of detrital zircons to infer
588 maximum depositional ages of strata: a test against a Colorado Plateau Mesozoic database. *Earth and*
589 *Planetary Science Letters* 288, 115-125, 2009.
- 590
- 591 Dinis, P.A., Fernandes, P., Jorge, R.C.G.S., Rodrigues, B., Chew, D.M. and Tassinari, C.G.: The
592 transition from Pangea amalgamation to fragmentation: constraints from detrital zircon geochronology on
593 West Iberia paleogeography and sediment sources. *Sedimentary Geology* 375, 172-187, 2018.



- 594
595 Domingos, L.C.G., Freire, J.L.S., Silva, F. G., Gonçalves, F., Pereira, E. and Ribeiro, A.: The Structure of
596 the Intramontane Upper Carboniferous Basins in Portugal. In: M. J. Lemos de Sousa, J.T. Oliveira (eds.),
597 The Carboniferous of Portugal. Memórias, Nova Série 29, Serviços Geológicos de Portugal, Lisboa: 187-
598 194, 1983.
599
600 Fedo, C.M., Sircombe, K.N. and Rainbird, R.H.: Detrital zircon analysis of the sedimentary record. In:
601 Zircon (eds. M. Hanchar & P.W.O. Hoskin) Reviews in Mineralogy and Geochemistry, 53, 277-303.
602 Mineral Society of America, Washington, DC, 2003.
603
604 Ferreira, P., Caldeira, R. and Calvo, R.: Geoquímica das rochas ígneas aflorantes na região de S. Matias,
605 Cuba (Alentejo). Comunicações Geológicas (2014) 101, Especial I, 93-97, 2014.
606
607 Fonseca, P., Munhá, J., Pedro, J., Rosas, F., Moita, P., Araújo, A. and Leal, N.: Variscan ophiolites and
608 high-pressure metamorphism in southern Iberia. *Ophioliti* 24, 259-268, 1999.
609
610 Frei, D. and Gerdes, A.: Precise and accurate in-situ U–Pb dating of zircon with high sample throughput
611 by automated LA-SF-ICP-MS. *Chemical Geology* 261(3-4): 261-27, 2009.
612
613 Gama, C., Pereira, M.F., Crowley, Q.G., Dias da Silva, Í. and Silva, J.B.: Detrital zircon provenance of
614 Triassic sandstone of the Algarve Basin (SW Iberia): Evidence of Gondwanan- and Laurussian-type
615 sources of sediment. *Geological Magazine*, in press.
616
617 Gehrels, G.E.: Detrital zircon U-Pb geochronology applied to tectonics. *Annual*
618 *Review of Earth and Planetary Sciences* 42: 127-149, 2014.
619
620 Gonçalves, F. and Carvalhosa, A.: Subsídios para o conhecimento geológico do Carbónico de Santa
621 Susana Vol. D' Hommage au géologue G. Zbyszewski. *Recherche de Civilisations*, Paris, pp. 109-130,
622 1984.
623
624 Gynn, J. and Gehrels, G.: Comparison of Detrital Zircon Age Distributions Using the K-S Test. Arizona
625 LaserChron Center. Available at: <https://laserchron.org/>, 2010
626
627 Jesus, A., Munhá, J., Mateus, A., Tassinari, C. and Nutman, A.: The Beja layered gabbroic sequence
628 (Ossa–Morena Zone, Southern Portugal): geochronology and geodynamic implications. *Geodinamica*
629 *Acta* 20, 139-157, 2007.
630
631 Jesus, A.P., Mateus, A., Munhá, J.M., Tassinari, C.G., Bento dos Santos, T.M. and Benoit, M.: Evidence
632 for underplating in the genesis of the Variscan synorogenic Beja
633 Layered Gabbroic Sequence (Portugal) and related mesocratic rocks. *Tectonophysics* 683: 148-171, 2016.



- 634
- 635 Lemos de Sousa, M.J. and Wagner, R.H.: General description of the terrestrial Carboniferous basins in
636 Portugal and history of investigations. In: Lemos de Sousa M.J. and Oliveira, J.T., (eds) The
637 Carboniferous of Portugal. Memórias dos Serviços Geológicos de Portugal 29:117-126, 1983.
- 638
- 639 Lima, S.M., Corfu, F., Neiva, A.M.R. and Ramos, M.F.: Dissecting complex magmatic processes: an in-
640 depth U-Pb study of the Pavia Pluton, Ossa-Morena Zone, Portugal. *Journal of Petrology* 53, 1887-1911,
641 2012.
- 642
- 643 Linnemann, U., Pereira, M.F., Jeffries, T., Drost, K. and Gerdes, A.: Cadomian orogeny and the opening
644 of the Rheic Ocean: new insights in the diachrony of geo-tectonic processes constrained by LA-ICP-MS
645 U–Pb zircon dating (Ossa-Morena and Saxo-Thuringian Zones, Iberian and Bohemian Massifs).
646 *Tectonophysics* 461, 21-43, 2008.
- 647
- 648 Lopes, G., Pereira, Z., Fernandes, P., Wicander, R., Matos, J.X., Rosa, D. and Oliveira, J.T.: The
649 significance of reworked palynomorphs (middle Cambrian to Tournaisian) in the Viséan Toca da Moura
650 Complex (South Portugal). Implications for the geodynamic evolution of Ossa Morena Zone. *Review of*
651 *Palaeobotany and Palynology* 200, 1-23, 2014.
- 652
- 653 Ludwig, K.R.: Isoplot/Ex Version 3.0: a Geochronological Toolkit for Microsoft Excel, 2003.
- 654
- 655 Machado, G., Dias da Silva, I. and Almeida, P.: Palynology, stratigraphy and geometry of the
656 Pennsylvanian continental Santa Susana Basin (SW Portugal). *Journal of Iberian Geology* 38, 429-448,
657 2012.
- 658
- 659 Moita, P., Santos, J.F. and Pereira, M.F.: Layered granitoids: interaction between continental crust
660 recycling processes and mantle-derived magmatism. Examples from the Évora Massif (Ossa-Morena
661 Zone, southwest Iberia, Portugal). *Lithos* 111, (3-4): 125-141, 2009.
- 662
- 663 Moita, P., Santos, J.F., Pereira, M.F., Costa, M.M. and Corfu, F.: The quartz-dioritic Hospitais intrusion
664 (SW Iberian Massif) and its mafic microgranular enclaves -evidence for mineral clustering. *Lithos* 224-
665 225, 78-100, 2015.
- 666
- 667 Oliveira, J.T., Oliveira, V. and Piçarra, J.: Traços gerais da evolução tectono-estratigráfica da Zona de
668 Ossa Morena, em Portugal. *Cuadernos do Laboratorio Xeoloxico de Laxe* 16, 221-250, 1991.
- 669
- 670 Pereira, M.F., Gama, C., Dias da Silva, Í., Fuenlabrada, J.M., Silva, J.B. and Medina, J.: Isotope
671 geochemistry evidence for Laurussian-type sources of South-Portuguese Zone Carboniferous turbidites
672 (Variscan orogeny). In: Murphy, J.B. (Eds). *Pannotia to Pangea: Neoproterozoic and Paleozoic orogenic*
673 *cycles in the circum-North Atlantic region*. Geological Society of London, Special Publication, in press.



- 674
675 Pereira, M.F., Martínez Poyatos, D., Pérez-Cáceres, I., Gama, C. and Azor, A.: Comment on
676 “Stratigraphy of the Northern Pulo do Lobo Domain, SW Iberia Variscides: A palynological
677 contribution” by Zélia Pereira et al. (2018) - *Geobios* 51, 491-506. *Geobios* 55: 103-106, 2019.
678
679 Pereira, M.F., Gutiérrez-Alonso, G., Murphy, J.B., Drost, K., Gama, C. and Silva, J.B.: Birth and demise
680 of the Rheic Ocean magmatic arc(s): Combined U-Pb and Hf isotope analyses in detrital zircon from SW
681 Iberia siliciclastic strata. *Lithos* 278-281, 383-399, 2017a.
682
683 Pereira, M.F., Gama, C. and Rodríguez, C.: Coeval interaction between magmas of contrasting
684 composition (Late Carboniferous-Early Permian Santa Eulália-Monforte massif, Ossa-Morena Zone):
685 field relationships and geochronological constraints. *Geologica Acta* 15, 409-428, 2017b.
686
687 Pereira, M.F., Chichorro, M., Moita, P., Santos, J.F., Solá, A.M.R., Williams, I.S., Silva, J.B. and
688 Armstrong, R.A.: The multistage crystallization of zircon in calc-alkaline granitoids: U-Pb age constraints
689 on the timing of Variscan tectonic activity in SW Iberia. *International Journal of Earth Sciences* 104, 5,
690 1167-1183, 2015a.
691
692 Pereira, M.F., Castro, A., Fernández, C.: The inception of a Paleotethyan magmatic arc in Iberia.
693 *Geosciences Frontiers*: 6, 297-306, 2015b.
694
695 Pereira, M.F., Ribeiro, C., Vilallonga, F., Chichorro, M., Drost, K., Silva, J.B., Albardeiro, L., Hofmann,
696 M. and Linnemann, U.: Variability over time in the sources of South Portuguese Zone turbidites:
697 evidence of denudation of different crustal blocks during the assembly of Pangea. *International Journal of*
698 *Earth Sciences*, 103, 1453-1470, 2014.
699
700 Pereira, M.F., Chichorro, M., Johnston, S., Gutiérrez-Alonso, G., Silva, J., Linnemann, U., Hofmann, M.
701 and Drost, K.: The missing Rheic ocean magmatic arcs: provenance analysis of Late Paleozoic
702 sedimentary clastic rocks of SW Iberia. *Gondwana Research* 22, 882-891, 2012a.
703
704 Pereira, M.F., Chichorro, M., Silva, J., Ordóñez-Casado, B., Lee, J. and Williams, I.: Early Carboniferous
705 wrenching, exhumation of high-grade metamorphic rocks and basin instability in SW Iberia; constrains
706 derived from structural geology and U-Pb and ⁴⁰Ar-³⁹Ar geochronology. *Tectonophysics* 558-559, 28-
707 44, 2012b.
708
709 Pereira, M.F., Solá, A.R., Chichorro, M., Lopes, L., Gerdes, A. and Silva, J.B.: North-Gondwana
710 assembly, break-up and paleogeography: U-Pb isotope evidence from detrital and igneous zircons of
711 Ediacaran and Cambrian rocks of SW Iberia. *Gondwana Research* 22(3-4): 866-881, 2012c.
712



713 Pereira, M.F., Chichorro, M., Williams, I.S., Silva, J.B., Fernandez, C., Diaz-Azpiroz, M., Apraiz, A. And
714 Castro, A.: Variscan intra-orogenic extensional tectonics in the
715 Ossa-Morena Zone (Évora-Aracena-Lora del Rio metamorphic belt, SW Iberian Massif): SHRIMP zircon
716 U-Th-Pb geochronology. In: Murphy, J.B., Keppie, J.D.,
717 Hynes, A.J. (Eds.), *Ancient Orogens and Modern Analogues* Geological Society,
718 London, Special Publications 327, 215-237, 2009.
719
720 Pereira, M.F., Chichorro, M., Williams, I.S. and Silva, J.B.: Zircon U-Pb geochronology of paragneisses
721 and biotite granites from the SW Iberia Massif. (Portugal): evidence for a paleogeographic link between
722 the Ossa-Morena Ediacaran basins and the West African craton. In: Ennih, N., Liégeois, J.P. (Eds.), *The*
723 *Boundaries of the West African Craton*. Geological Society Special Publication, London 297, 385-408,
724 2008.
725
726 Pereira, M.F., Silva, J.B., Chichorro, M., Moita, P., Santos, J.F., Apraiz, A. and Ribeiro, C.: Crustal
727 growth and deformational processes in the Northern Gondwana margin:
728 constraints from the Évora Massif (Ossa-Morena Zone, SW Iberia, Portugal). In: Linnemann, U., Nance,
729 R.D., Kraft, P., Zulauf, G. (Eds.), *The evolution of the Rheic*
730 *Ocean: from Avalonian–Cadomian active margin to Alleghenian-Variscan Collision* Special Paper of the
731 *Geological Society of America* 423, 333-358, 2007.
732
733 Pereira, M.F., Chichorro, M., Linnemann, U., Eguiluz, L. and Silva, J.B.: Inherited arc signature in
734 Ediacaran and Early Cambrian basins of the Ossa-Morena Zone (Iberian Massif, Portugal):
735 Paleogeographic link with European and North African correlatives.
736 *Precambrian Research* 144, 297-315, 2006.
737
738 Pérez-Cáceres, I., Poyatos, D.M., Simancas, J.F. and Azor, A.: Testing the Avalonian affinity of the South
739 Portuguese Zone and the Neoproterozoic evolution of SW Iberia through detrital zircon populations.
740 *Gondwana Research* 42, 177-192, 2017.
741
742 Pérez-Cáceres, I., Martínez Poyatos, D., Simancas, J.F. and Azor, A.: The elusive nature of the Rheic
743 Ocean suture in SW Iberia, *Tectonics*, 34, 2429-2450, 2015.
744
745 Pin, Ch., Fonseca, P.E., Paquette, J.L., Castro, P. and Matte, Ph.: The ca. 350 Ma Beja igneous complex:
746 a record of transcurrent slab break-off in the southern Iberia Variscan Belt? *Tectonophysics* 461, 356-377,
747 2008.
748
749 Priem, H.N.A., Boelrijk, N.A.I.M., Hebeda, E.H. and Schermerhorn, L.J.G.: Isotopic ages of the
750 Alcáçovas orthogneiss and the Beja porphyries, South Portugal. *Comunicações Serviços Geológicos*
751 *Portugal* 72: 3-7, 1986.
752



- 753 Quesada, C. and Oliveira, J.T.: The Geology of Iberia: A Geodynamic Approach. Volume 2: The
754 Variscan Cycle (Simas, F., volume coordinator). Regional Geology Reviews, Springer, p. 1-542, 2019.
755
- 756 Quesada, C., Fonseca, P.E., Munha, J., Oliveira, J.T. and Ribeiro, A.: The Beja–Acebuches Ophiolite
757 (Southern Iberia Variscan fold belt): geological characterization and significance. Boletín Geológico y
758 Minero 105, 3-49, 1994.
759
- 760 Quesada, C., Robardet, M. and Gabaldon, V.: Ossa-Morena Zone. Stratigraphy. Synorogenic phase
761 (Upper Devonian-Carboniferous-Lower Permian). In: Dallmeyer, R.D., Martínez García, E. (Eds.), Pre-
762 Mesozoic Geology of Iberia. Springer-Verlag, Berlin-Heidelberg, 273-279, 1990.
763
- 764 Ribeiro, A., Munhá, J., Dias, R., Mateus, A., Pereira, E., Ribeiro, L., Fonseca, P., Araújo, A., Oliveira, T.,
765 Romão, J., Chaminé, H., Coke, C. and Pedro, J.: Geodynamic evolution of the SW Europe Variscides.
766 Tectonics 26, TC6009, <https://doi.org/10.1029/2006TC002058>, 2007.
767
- 768 Rodrigues, B., Chew, D.M., Jorge, R.C.G.S., Fernandes, P., Veiga-Pires, C. & Oliveira, J.T.: Detrital
769 zircon geochronology of the Carboniferous Baixo Alentejo Flysch Group (South Portugal); constraints on
770 the provenance and geodynamic evolution of the South Portuguese Zone. Journal of the Geological
771 Society of London, <http://dx.doi.org/10.1144/jgs2013-084>, 2014.
772
- 773 Rosas, F.M., Marques, F.O., Balleve, M. and Tassinari, C.: Geodynamic evolution of the SW Variscides:
774 orogenic collapse shown by new tectonometamorphic and isotopic data from western Ossa-Morena Zone,
775 SW Iberia. Tectonics 27, TC0080. <https://doi.org/10.1029/2008TC002333>, 2008.
776
- 777 Santos, J., Mata, J., Gonçalves, F. and Munhá, J.: Contribuição para o conhecimento Geológico-
778 Petrológico da Região de Santa Susana: O Complexo Vulcano-sedimentar da Toca da Moura.
779 Comunicações dos Serviços Geológicos de Portugal 73 (1-2), 29-48, 1987.
780
- 781 Santos, J.F., Andrade, A.S. and Munhá, J.: Magmatismo orogénico Varisco no limite meridional da Zona
782 de Ossa-Morena. Comunicações dos Serviços Geológicos de Portugal, 76, 91-124, 1990.
783
- 784 Simancas, J.F., Tahiri, A., Azor, A., González Lodeiro, F., Martínez Poyatos, D. and El Hadi, H.: The
785 tectonic frame of the Variscan-Alleghanian orogen in southern Europe and northern Africa.
786 Tectonophysics 398, 181-198, 2005.
787
- 788 Simancas, J.F., Azor, A., Martínez Poyatos, D.J., Tahiri, A., El Hadi, H., González-Lodeiro, F., Pérez-
789 Estaún, A. and Carbonell, R.: Tectonic relationships of Southwest Iberia with the allochthons of
790 Northwest Iberia and the Moroccan Variscides. *Compte Rendus Geoscience* 341, 103-113, 2009.
791



- 792 Spencer, C.J., Kirkland, C.L., and Taylor, R.J.M.: Strategies towards statistically robust interpretations of
793 in situ U-Pb zircon geochronology. *Geoscience Frontiers* 7, 581-589, 2015.
794
- 795 Teixeira, C.: Sobre a flora fossil do Carbónico alentejano. *Boletim do Museu do Laboratório de geologia,*
796 *Universidade de Lisboa, 3ª série, 7-8: 83-100, 1938-1940.*
797
- 798 Teixeira, C.: Sur quelques insectes fossiles du Carbonifere de l'Alentejo. *Anais Faculdade de Ciências,*
799 *Porto, vol. XXVI, 2: 117-120, 1941.*
800
- 801 Teixeira, C.: O Antracólítico continental português. (Estratigrafia- Tectónica). *Boletim da Sociedade*
802 *Geológica, porto, vol. 5, Fasc.1-2: 1-139, 1944.*
803
- 804 Vermeesch, P.: Multi-sample comparison of detrital age distributions. *Chemical Geology* 341, 140-146,
805 2013.
806
- 807 Vermeesch, P.: IsoplotR: A free and open toolbox for geochronology. *Geoscience Frontiers* 9, 5, 1479-
808 1493, 2018
809
- 810 Wagner, R.H. and Lemos de Sousa, M.J.: The Carboniferous megaflores of Portugal-a revision of
811 identifications and discussion of stratigraphic ages. In: Sousa, M.J.L., Oliveira, J.T. (Eds.), *The*
812 *Carboniferous of Portugal. Memórias dos Serviços Geológicos de Portugal, Lisboa, pp. 127-152, 1983.*
813
- 814 Wissink G.K., Wilkinson, B.H., and Hoke, G.D: Pairwise sample comparisons and multidimensional
815 scaling of detrital zircon ages with examples from the North American platform, basin, and passive
816 margin settings. *Lithosphere* 10, 3, 478-491, 2018.
817
- 818 **Figure captions**
- 819 Figure 1: A- Inset with location of SW Iberia in the Iberian Variscan belt with regional
820 distribution of the main Paleozoic terranes: CIZ- Central Iberian Zone; CZ- Cantabrian Zone;
821 GTMZ- Galicia-Trás-os-Montes Zone; OMZ- Ossa-Morena Zone; PLZ- Pulo do Lobo Zone;
822 SPZ- South-Portuguese Zone and WALZ- West Asturian-Leonese Zone. B- Simplified
823 Geological Map of SW Iberia showing the South-Portuguese, Pulo do Lobo and Ossa-Morena
824 zones (Modified from Pereira et al. 2017a, 2019 and references therein; Quesada and Oliveira,
825 2019).
826
- 827 Figure 2: Simplified geological map and schematic stratigraphy of the Santa Susana-São
828 Cristovão region (Ossa-Morena Zone; Modified from Gonçalves and Carvalhosa, 1984;
829 Machado et al., 2012). Sampling locations of the Carboniferous sedimentary and igneous rocks
830 used for geochronology are indicated with yellow stars.



831

832 Figure 3: Photographs of the Carboniferous igneous rocks of the Santa Susana-São Cristovão
833 region: A- Baleizão porphyry intrusive contact (yellow arrow) with siliciclastic rocks of the
834 Toca da Moura volcano-sedimentary complex; B- Baleizão porphyry; C-D- Rhyolitic tuffs of
835 the Toca da Moura volcano-sedimentary complex; E- Volcanic breccia with fragments of
836 siltstone (black) and rhyolite (yellow) at the base of the silicic tuffs from the Toca da Moura
837 volcano-sedimentary complex; F- Pillow-lava of andesitic basalt-to-basalt intercalated in the
838 siliciclastic rocks of the Toca da Moura volcano-sedimentary complex.

839

840 Figure 4: Photographs of the Carboniferous sedimentary rocks of the Santa Susana Formation
841 lower member: A- View of dipping meter-thick beds of medium-coarse grained sandstone
842 intercalated with conglomerate; B- Planar-bedded coarse-grained sandstone; C- Plant imprints
843 in sandstone; D- Conglomerate with cobbles and pebbles of granite (G), quartzite (Q), silicic
844 porphyry (SP) and mafic volcanic rock (M); E- Conglomerate with pebbles of rhyolite (R),
845 phyllite (P), felsic tuff (T) and quartzite (Q).GG

846

847 Figure 5: Petrographic images of the Carboniferous sedimentary and igneous rocks of the Santa
848 Susana-São Cristovão region: A- Rhyolitic-rhyodacitic tuff of the Toca da Moura volcano-
849 sedimentary complex showing quartz and feldspar phenocrysts enclosed in ash matrix; B-
850 Rhyolitic tuff showing flattened dark-brown millimeter-sized pumice and lithoclasts enclosed in
851 ash matrix; C- Porphyritic texture of the Baleizão rhyodacite-rhyolite characterized by quartz,
852 plagioclase, K-feldspar, biotite and amphibole phenocryst embedded in a fine-grained silicic
853 matrix; D- Cobble of fine-grained granite showing graphic intergrowths of quartz and alkali
854 feldspar, found in conglomerate from the Santa Susana Formation; E- Siltstone of the Toca da
855 Moura volcano-sedimentary complex mostly composed of quartz grains and a few grains of
856 plagioclase (P), tourmaline (T), and rock fragments (L); F- Siltstone of the Cabrela volcano-
857 sedimentary complex showing fining upwards grading and a slump-fold; G-H, Sandstones from
858 the Santa Susana Formation with high percentage of lithoclasts (L) and a few feldspar (F).

859

860 Figure 6: Concordia diagrams, weighted mean of $^{206}\text{Pb}/^{238}\text{U}$ ages of analyzed zircon grains
861 extracted from silicic tuffs of the Toca da Moura volcano-sedimentary complex.

862

863 Figure 7: Concordia diagrams, weighted mean of $^{206}\text{Pb}/^{238}\text{U}$ ages of analyzed zircon grains of:
864 A- the Baleizão porphyry and B- the cobble of granite found in conglomerate from the Santa
865 Susana Formation.

866



867 Figure 8: Pie diagrams and Kernel Density Estimation (KDE) with U-Pb detrital-zircon ages of
868 siliciclastic rocks from: A- the Toca da Moura (TM-3, this study) and Cabrela (CB: CBR-11,
869 this study; and OM-200, Pereira et al., 2012a) volcano-sedimentary complexes, and B- the Santa
870 Susana Formation (SS-1 and SS-2, this study; and SS Upper member, StSz2 and StSz4 from
871 Dinis et al., 2018); C- U-Pb age cumulative frequency plots applied to the U-Pb ages (90-110%
872 concordance) of detrital zircon grains from the Toca da Moura and Cabrela volcano-
873 sedimentary complexes, and the Santa Susana Formation.

874

875 Figure 9: A- Results of the K-S (Kolmogorov-Smirnov) test and B- Multi-Dimensional Scaling
876 diagrams (Vermeesch, 2018) applied to the U-Pb ages (90-110% concordance) of detrital zircon
877 grains from the Toca da Moura (TM-3) and Cabrela (CB) volcano-sedimentary complexes, and
878 the Santa Susana Formation (SS1, SS2, SS upper member), and different potential sources:
879 OMZ (Linnemann et al. 2008; Pereira et al. 2008, 2012c), PLZ (Pereira et al. 2017; Pérez
880 Cáceres et al. 2017), SPZ (Braid et al. 2011; Pereira et al., 2012a, 2014; Rodrigues et al. 2014).
881 Abbreviations: MT- Mértola Formation; MR- Mira formation; BJ- Brejeira formation; PQ-
882 TRC- Phyllite-Quartzite and Tercenas formations; SI-REP- Santa Iria and Represa formations;
883 P-G-R-A-R- Pulo do Lobo, Gafo, Ribeira de Lima, Atalaia and Ronquillo formations; HT-
884 Horta da Torre Formation.

885

886 Figure 10: Sketches showing inferred tectonic evolution and sedimentation recorded in SW
887 Iberia Carboniferous stratigraphy during Laurussian-Gondwana oblique collision; A- Early
888 Carboniferous; B- Late Carboniferous.

889

890

891

892

893

894

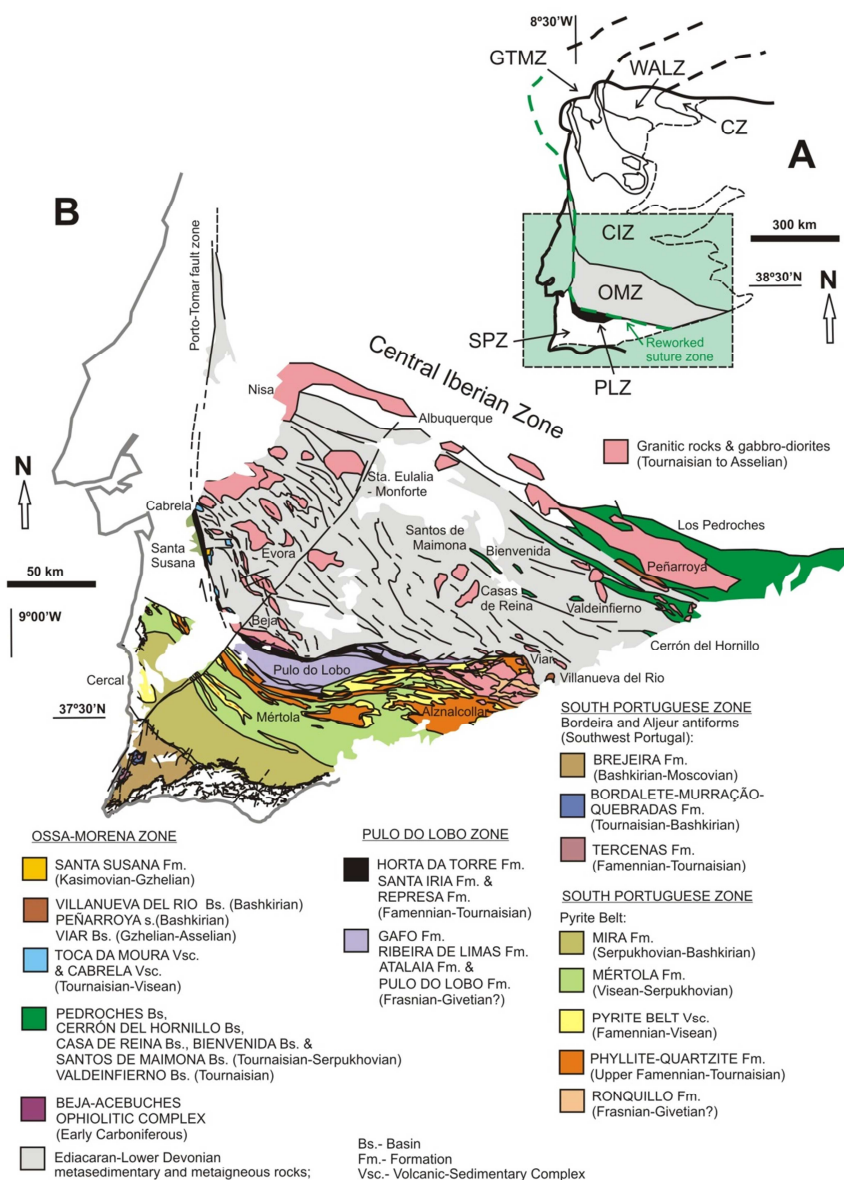


Figure 1

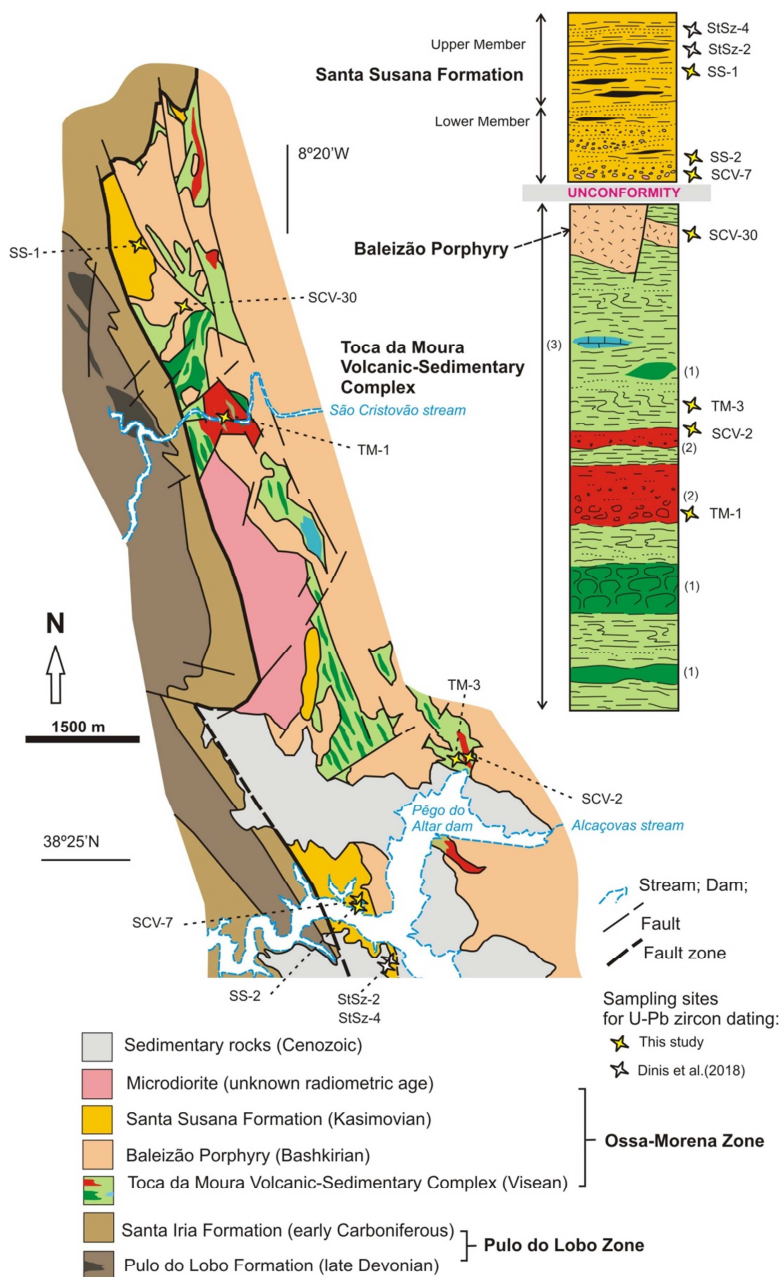


Figure 2

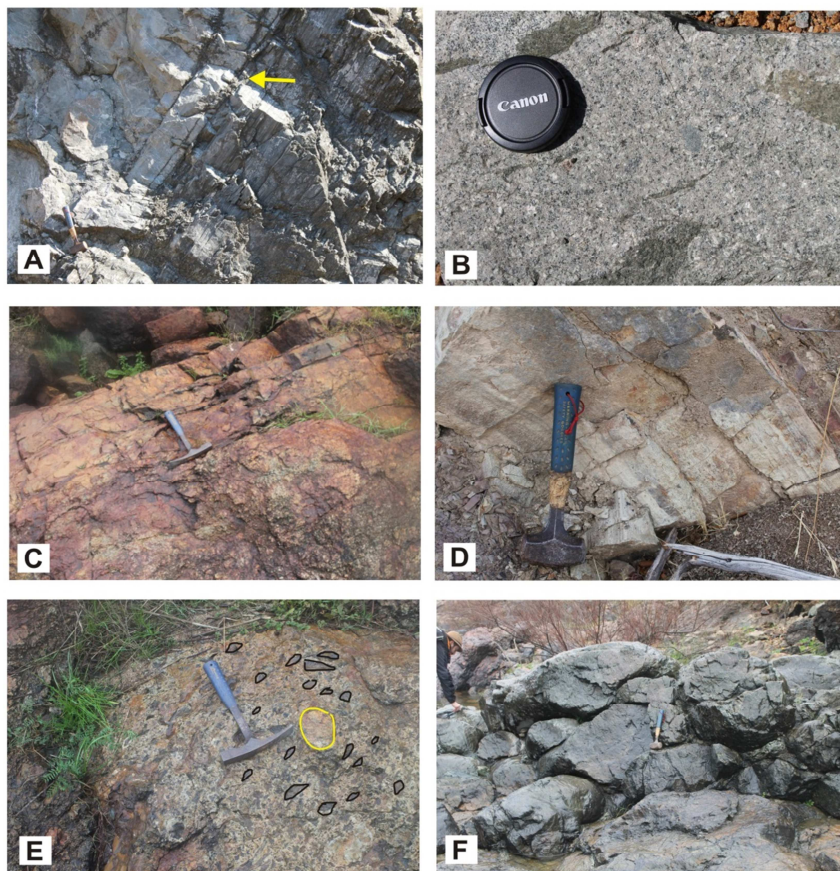


Figure 3

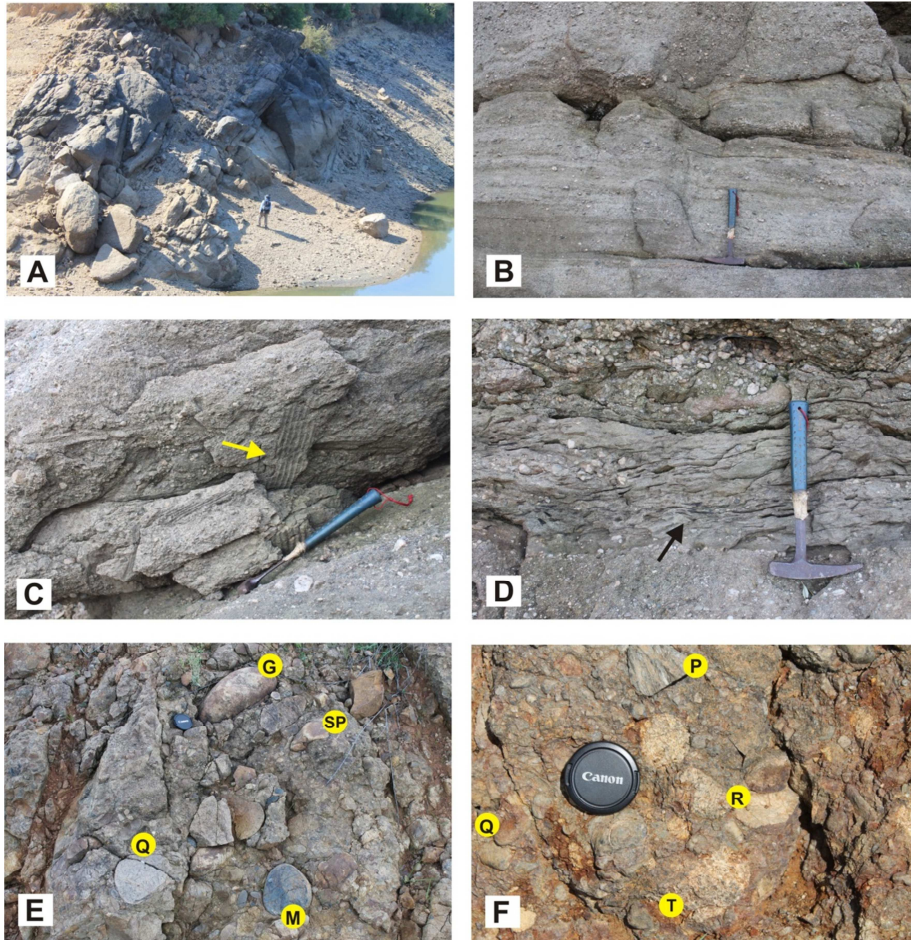


Figure 4

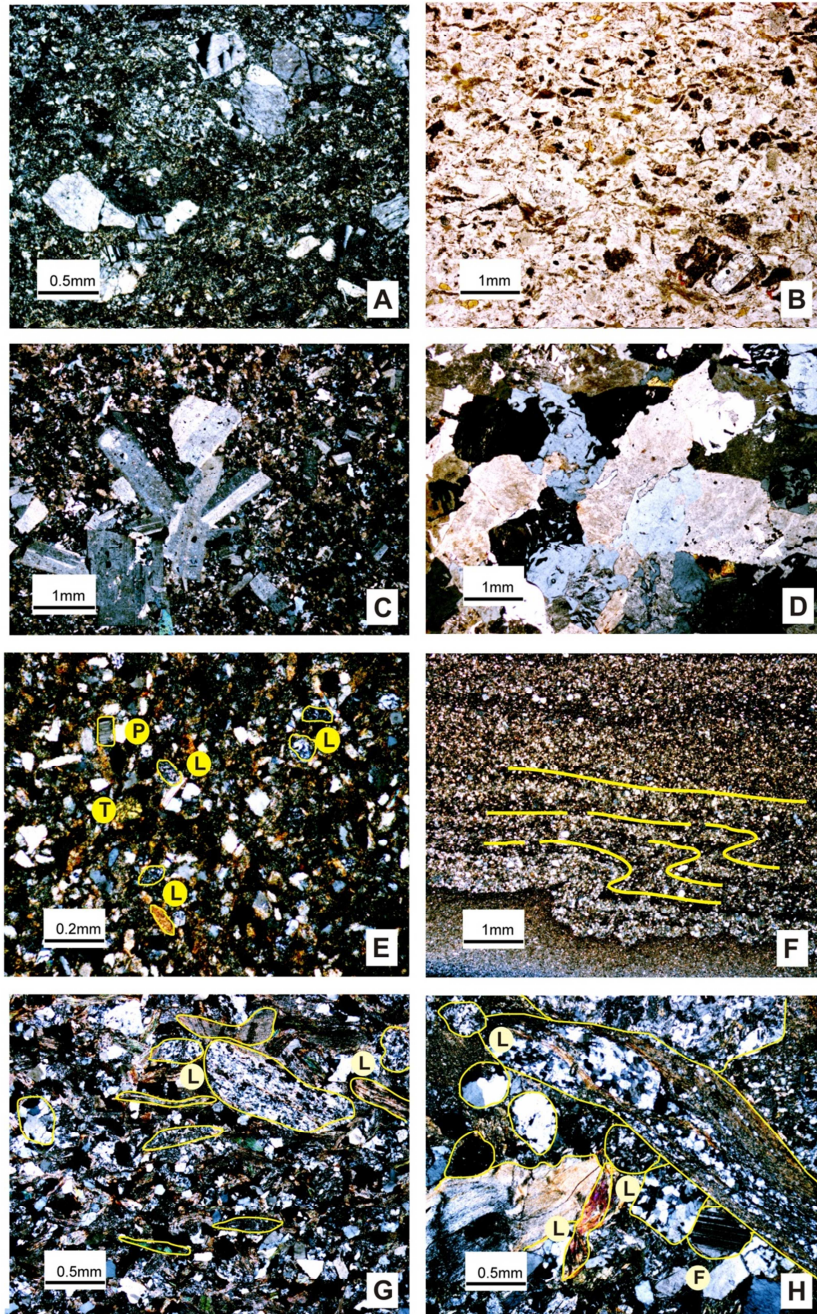


Figure 5

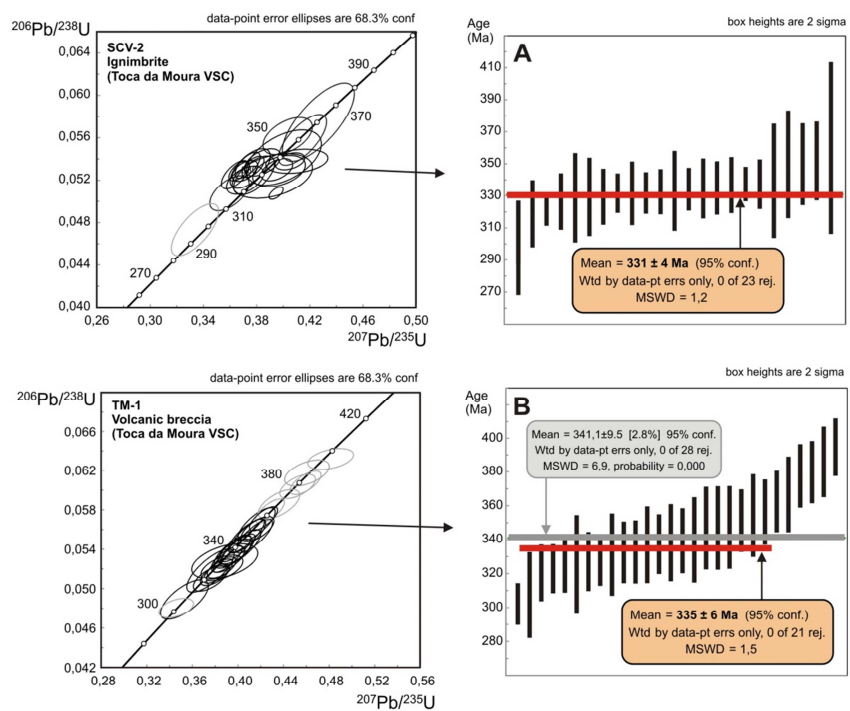


Figure 6

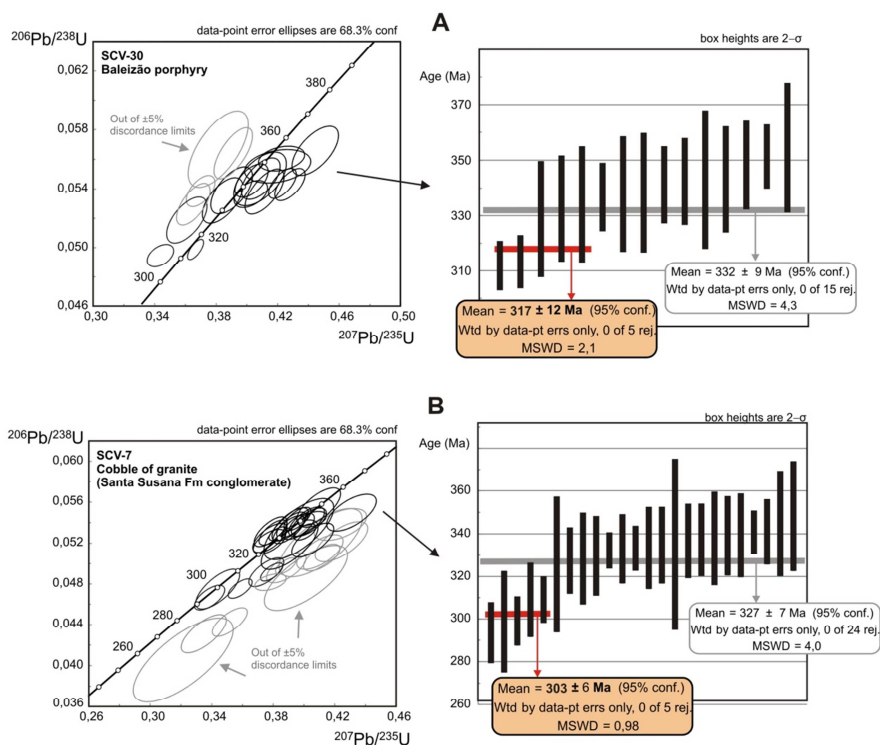


Figure 7

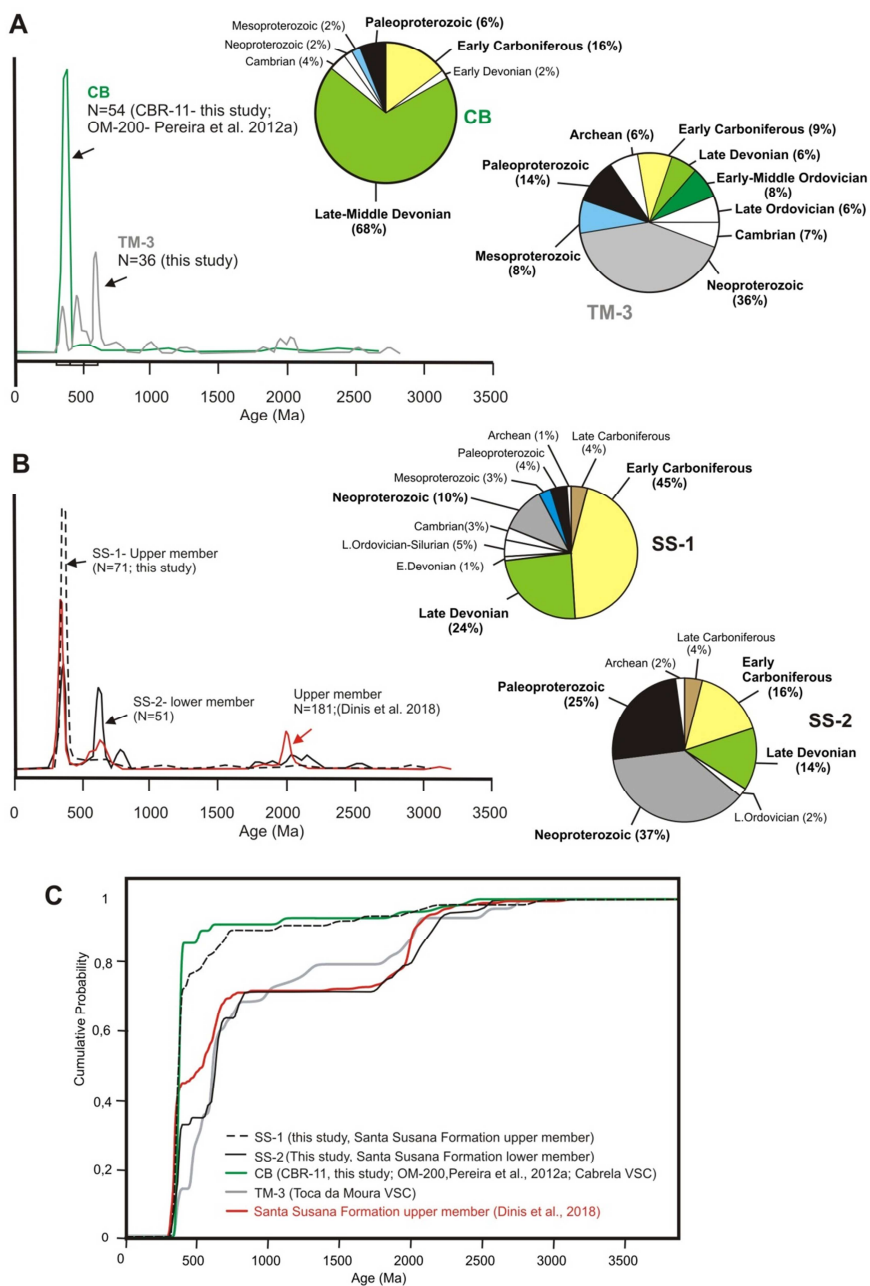


Figure 8



A Kolmogorov-Smirnov Test

All ages

| | TM-3 | CB | SS1 | SS2 | SS upper mb. | MT | MR | BJ | PQ-TRC | SI-REP | P-G-R-A-R | HT | OMZ |
|--------------|-------|-------|-------|-------|--------------|-------|-------|-------|--------|--------|-----------|-------|-------|
| TM-3 | | 0.000 | 0.000 | 0.391 | 0.004 | 0.000 | 0.761 | 0.458 | 0.496 | 0.308 | 0.003 | 0.000 | 0.003 |
| CB | 0.731 | | 0.003 | 0.000 | 0.000 | 0.158 | 0.000 | 0.000 | 0.000 | 0.000 | 0.000 | 0.000 | 0.000 |
| SS1 | 0.637 | 0.330 | | 0.000 | 0.000 | 0.049 | 0.000 | 0.000 | 0.000 | 0.000 | 0.000 | 0.000 | 0.000 |
| SS2 | 0.195 | 0.552 | 0.465 | | 0.163 | 0.000 | 0.856 | 0.001 | 0.038 | 0.756 | 0.000 | 0.000 | 0.000 |
| SS Upper mb. | 0.323 | 0.412 | 0.323 | 0.176 | | 0.000 | 0.000 | 0.000 | 0.000 | 0.000 | 0.000 | 0.000 | 0.000 |
| MT | 0.608 | 0.183 | 0.200 | 0.511 | 0.358 | | 0.000 | 0.000 | 0.000 | 0.000 | 0.000 | 0.000 | 0.000 |
| MR | 0.122 | 0.617 | 0.522 | 0.096 | 0.215 | 0.538 | | 0.000 | 0.004 | 0.000 | 0.000 | 0.000 | 0.000 |
| BJ | 0.150 | 0.806 | 0.691 | 0.285 | 0.406 | 0.675 | 0.193 | | 0.109 | 0.000 | 0.000 | 0.000 | 0.000 |
| PQ-TRC | 0.145 | 0.715 | 0.620 | 0.210 | 0.357 | 0.656 | 0.160 | 0.091 | | 0.000 | 0.000 | 0.000 | 0.000 |
| SI-REP | 0.168 | 0.568 | 0.508 | 0.167 | 0.323 | 0.514 | 0.199 | 0.245 | 0.177 | | 0.000 | 0.000 | 0.000 |
| P-G-R-A-R | 0.304 | 0.871 | 0.781 | 0.336 | 0.473 | 0.818 | 0.292 | 0.173 | 0.163 | 0.308 | | 0.000 | 0.000 |
| HT | 0.492 | 0.867 | 0.754 | 0.522 | 0.524 | 0.779 | 0.558 | 0.501 | 0.515 | 0.589 | 0.477 | | 0.000 |
| OMZ | 0.309 | 0.876 | 0.790 | 0.352 | 0.481 | 0.824 | 0.298 | 0.163 | 0.194 | 0.359 | 0.168 | 0.480 | |

D-values using error in the CDF

Pre-Carboniferous ages

| | TM-3 | CB | SS1 | SS2 | SS upper mb. | MT | MR | BJ | PQ-TRC | SI-REP | P-G-R-A-R | HT | OMZ |
|--------------|-------|-------|-------|-------|--------------|-------|-------|-------|--------|--------|-----------|-------|-------|
| TM-3 | | 0.000 | 0.003 | 0.411 | 0.074 | 0.000 | 0.044 | 0.397 | 0.398 | 0.487 | 0.003 | 0.000 | 0.003 |
| CB | 0.712 | | 0.015 | 0.000 | 0.000 | 0.000 | 0.000 | 0.000 | 0.000 | 0.000 | 0.000 | 0.000 | 0.000 |
| SS1 | 0.427 | 0.347 | | 0.001 | 0.000 | 0.516 | 0.000 | 0.000 | 0.000 | 0.003 | 0.000 | 0.000 | 0.000 |
| SS2 | 0.203 | 0.696 | 0.451 | | 0.870 | 0.000 | 0.715 | 0.388 | 0.652 | 0.068 | 0.168 | 0.000 | 0.113 |
| SS Upper mb. | 0.246 | 0.734 | 0.452 | 0.109 | | 0.000 | 0.020 | 0.000 | 0.001 | 0.000 | 0.004 | 0.000 | 0.002 |
| MT | 0.492 | 0.243 | 0.161 | 0.608 | 0.606 | | 0.000 | 0.000 | 0.000 | 0.000 | 0.000 | 0.000 | 0.000 |
| MR | 0.257 | 0.779 | 0.496 | 0.121 | 0.191 | 0.644 | | 0.205 | 0.044 | 0.000 | 0.036 | 0.000 | 0.038 |
| BJ | 0.158 | 0.795 | 0.459 | 0.149 | 0.231 | 0.606 | 0.105 | | 0.182 | 0.000 | 0.000 | 0.000 | 0.000 |
| PQ-TRC | 0.169 | 0.719 | 0.458 | 0.121 | 0.211 | 0.616 | 0.135 | 0.082 | | 0.000 | 0.000 | 0.000 | 0.000 |
| SI-REP | 0.145 | 0.573 | 0.313 | 0.213 | 0.281 | 0.471 | 0.312 | 0.235 | 0.180 | | 0.000 | 0.000 | 0.000 |
| P-G-R-A-R | 0.306 | 0.856 | 0.599 | 0.178 | 0.178 | 0.757 | 0.125 | 0.162 | 0.141 | 0.289 | | 0.000 | 0.000 |
| HT | 0.491 | 0.848 | 0.633 | 0.454 | 0.352 | 0.721 | 0.499 | 0.496 | 0.507 | 0.581 | 0.478 | | 0.000 |
| OMZ | 0.309 | 0.862 | 0.597 | 0.194 | 0.196 | 0.755 | 0.131 | 0.151 | 0.182 | 0.350 | 0.167 | 0.479 | |

D-values using error in the CDF

Legend:
 P-value > 0.05: "not significantly different" (green)
 0.05 > P-value > 0.001: "not enough significantly different" (yellow)
 P-value < 0.001: "significantly different" (white)

MDS diagrams

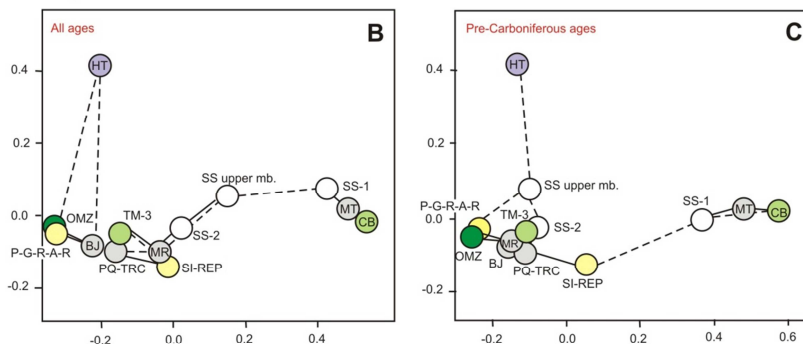


Figure 9

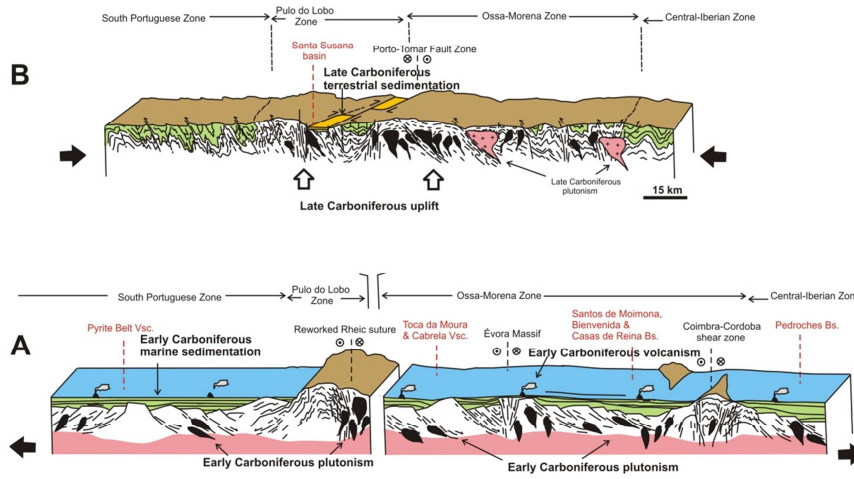


Figure 10